Model Updating Based on MDOF Transmissibility Concept

Francisco Roquette Quadros Saldanha

Thesis to obtain the Master of Science Degree in

Aerospace Engineering

Supervisor: Prof. Miguel António Lopes de Matos Neves

Examination Committee

Chairperson: Prof. Filipe Szolnoky Ramos Pinto Cunha
Supervisor: Prof. Miguel António Lopes de Matos Neves
Member of the Committee: Prof. Tiago Alexandre Narciso da Silva

November 2016

Acknowledgments

I would like to express my sincere acknowledgements to Professor Miguel de Matos Neves for the opportunity to do this work under his guidance and for his endless support, availability and motivation throughout the development of this thesis.

Resumo

O ajustamento de modelos pode ser visto como uma introdução de correcções nos parâmetros do modelo de forma a aproximar a resposta numérica do modelo à resposta experimental. Um exemplo com interesse para este trabalho é o ajuste de parâmetros de modelos de elementos finitos (EF) à luz de resultados obtidos experimentalmente. Este trabalho aborda o problema de ajustamento de modelos de EF com o desenvolvimento de uma metodologia baseada no conceito de transmissibilidade para modelos com múltiplos graus de liberdade (MGDL). As metodologias de ajustamento de modelos de EF desenvolvidos, baseadas nas funções de resposta em frequência (FRF) e transmissibilidade (TR), são implementadas e testadas utilizando resultados experimentais obtidos de duas estruturas, uma viga e uma estrutura muito simplificada de uma aeronave. Comparando os resultados experimentais com os resultados correspondentes obtidos do modelo de EF final ajustado, é concluído que ambas as metodologias funcionam adequada e eficientemente, de tal forma que na maior parte das simulações de ajustamento dos modelos numéricos efectuadas foi alcançada um sobreposição entre os valores correspondentes aos resultados experimentais e numéricos, bastante adequada. No entanto, é também possível verificar que as estimativas finais do processo de ajustamento para os parâmetros ajustados não são únicas, mas sim dependentes, entre outras variáveis, do número de parâmetros escolhidos em cada simulação e da escolha dos parâmetros propriamente dita.

Palavras-chave: ajustamento de modelos, resposta em frequência, transmissibilidade, correlação, viga de Timoshenko

Abstract

Model updating can be seen as the introduction of corrections at parameters of the model to improve the approximation of the model response to the experimental response. An example with interest for this work is the adjustment of Finite Element (FE) models in the light of experimental data. This work addresses the model updating issue with the development of a model updating procedure based on the Multi-Degree of Freedom (MDOF) Transmissibility (TR) concept. The developed FE model updating methodologies, based on the frequency response functions (FRFs) and TR correlation functions, are implemented and tested using experimental testing data from a simple beam and an aircraft-like structure. Comparing the experimental data obtained from structural testing with the corresponding numerical data from the final updated FE model, it is concluded that both updating procedures work rather effectively, so that in most updating simulations performed, a quite adequate fit between the experimental and numerical data is achieved. However, it is also verified that the updating parameter estimates are not unique, but dependent on the selection and number of updating parameters considered, among other variables.

Keywords: model updating, frequency response function, transmissibility, correlation, Timoshenko beam theory.

Contents

List of Tables

List of Figures

Nomenclature

Operators and Matrix Notation

$[\,]^{+}$ pseudo-inverse of a matrix

$[\,]^{H}, \{\}^{H}$ complex conjugate (Hermitian) transpose of a matrix, column vector

$[\,]^{T}, \{\}^{T}$ transpose of a matrix, column vector

$[\,]^{-1}$ inverse of a square matrix

$\begin{bmatrix} \ddots & \\ & \ddots \end{bmatrix}$ diagonal matrix

$|.|$ absolute Value

$|Z|$ determinant of matrix Z

Basic Terms and Subscripts

$[0], \{0\}$ null matrix, column vector

$\begin{bmatrix} \ddots & & \\ & I & \\ & & \ddots \end{bmatrix}$ identity matrix

$\imath$ imaginary unit, $\sqrt{-1}$

ω frequency of vibration $[rad/s]$

ω_r r^{th} frequency point $[rad/s]$

$\{\dot{x}(t)\}, \{\ddot{x}(t)\}$ 1st and 2nd time derivatives of displacement

$\{f(t)\}$ time varying excitation force vector

$\{F\}$ amplitude of excitation force vector

$\{x(t)\}$ time varying displacement vector

$\{X\}$ amplitude of displacement vector

i, j, k, l running indices

N number of DOFs in FE model

N_e number of DOFs in a single FE

N_f number of frequency points

r mode number

t time variable

Model Properties and Modal Parameters

$[M], [K], [C]$ mass, stiffness and viscous damping matrices

$[M]_e, [K]_e, [C]_e$ elemental mass, stiffness and viscous damping matrices

$[Z(\omega)]$ general impedance matrix

α mass proportional (Rayleigh) damping coefficient

β stiffness proportional (Rayleigh) damping coefficient

λ_r eigenvalue of the rth mode

$\left[\lambda_r\right]$ eigenvalue matrix

$\left[\Phi\right]$ mass-normalized mode shape matrix

$\left[\Psi\right]$ mode shape/eigenvector matrix

ω_r natural frequency of the rth mode $[rad/s]$

ξ_r viscous damping ratio of the rth mode

$\{\psi\}_r, \{\phi\}_r$ r^{th} mode shape/eigenvector

k_r modal/effective stiffness of the rth mode

m_r modal/effective mass of the rth mode

Response and Transmissibility Properties

$[\alpha(\omega)], [Y(\omega)], [A(\omega)]$ receptance, mobility, accelarance matrix

$\{H(\omega)\}$ general frequency response function matrix

$\{H_{ij}(\omega)\}$ frequency response vector, response DOF i, excitation DOF j, all N_f frequency points

$\{T_{ij}(\omega)\}$ transmissibility vector, TR of force to DOF i, from DOF j, all N_f frequency points

$\{X_i(\omega)\}$ response spectra vector, response DOF j, all N_f frequency points

$CSAC(\omega_r)$ cross signature assurance criterion correlation function, frequency point k

$CSF(\omega_r)$ cross signature scale factor correlation function, frequency point k

List of Abbreviations

3D 3-dimentional. 9, 32, 38, 51, 56

BC Bondary Condition. 8, 9, 16, 17, 26, 31, 38, 75

CSAC Cross Signature Assurance Criterion. 20

CSC Cross Signature Correlation. 20

CSF Cross Signature Scale Factor. 20

dB Decibel. 34

DOF Degree Of Freedom. 9–11, 38, 43, 53, 56

EOM Equation Of Motion. 10

FE Finite Element. v, xi, xii, 1–3, 5, 7, 9, 16, 20, 23, 25–28, 31–34, 38, 39, 43, 50–52, 55–57, 64, 67, 68

FRAC Frequency Response Assurance Criterion. 20

FRF Frquency Response Functions. xi, 2, 3, 11–15, 20, 23, 26, 31, 37, 39, 40, 45

MAC Modal Assurance Criterion. 20

MDOF Multi-Degree Of Freedom. v, xi, 14, 15

NDOF Number of Degrees Of Freedom. 9

TR Transmissibility. v, xi, 2, 3, 14, 17, 21, 23, 26, 31, 34–37, 48, 67

Chapter 1

Introduction

1.1 Problem Statement and Motivation

In the field of structural dynamics, engineers are constantly challenged to design increasingly complex products that must satisfy more stringent criteria. Essentially, products must be quieter, safer, lighter more reliable as well as less expensive to build and maintain.

With the development and incorporation of developing computerized simulation tools as part of the design cycle of products, companies operating in the engineering industry expect to keep development times and cost competitive.

Extensive Finite Element FE calculation times are still an issue despite the fast development of computers in terms of performance. The arising question is how to replace large and complex FE models for smaller models, without loosing much accuracy.

If the relationship between input (design parameters) and the desired output can be design with acceptable accuracy, the high computational time problem can be overcome using the so-called “meta-model”, imposing the model updating procedures in order to guarantee the necessary predictive capabilities of the approximate model.

At the conception level of a product, the earlier a physical system and a mathematical model are available, the earlier a new and improved version of the final product can be achieved. The main purpose of such updated numerical models is to predict both the response of the system under specific loading conditions and the consequent design advantage obtained from eventual modifications in the configuration of the structure [1].

Missing knowledge on material properties parameters, lack of proper models for complex structures or connections or even just inaccurate parameters for the model formulation, introduce discrepancies between the experimental and the numerical models responses. Model Updating targets to modify the stiffness, mass and damping parameters of the system in order to get a better correlation between the numerical response and test data [1].

Most often, FE model updating procedures make use of modal data, such as eigenfrequencies and mode shapes. However, extensive research has been performed in updating FE models directly from

frequency response functions (FRFs) data. An example of FE model updating using FRF correlation functions is presented in [2]. Steenackers and his co-workers in [3] propose a new FE model updating methodology from output-only transmissibilitiy (TR) measurements, applying a regressive optimization technique.

Aerospace engineering is one of the most competitive industries, combining the state of the art in simulation techniques with extremely strict design performance requirements. Such requirements commonly arise from economic and environmental aspects but also from norms and regulations imposed by governing bodies to ensure that the established safety standards are satisfied.

The accurate prediction of the dynamic structural response of spacecraft structures during the most crucial stages of flight such as lunch and ascend as well as precision landing, is a major concern in the design and verification stages, thus requiring accurate mathematical models [4].

Therefore, it is mandatory that these numerical models which represent the real structures have a defined level of accuracy. Structural general requirements and definition of levels of accuracy for space engineering structures are defined in [5].

In the paper [6], Brughmans and his co-workers discuss the application of a FE model updating technique based on a forward sensibility formulation, to a twin propeller commuter aircraft , the Boeing DeHavilland DASH 8-300A aircraft, using ground vibration test data.

In [4], two example are used for demonstrating the applicability of a model updating technique to complex aerospace structures. In [7, 8], some examples of model validation using experimental data are analyzed, describing structures including an aeroengine and a civil aircraft structure.

1.2 Objectives of this Thesis

FE model updating procedures can be seen as an optimization problem in which the discrepancies between the numerical and experimental data are minimized by adjusting the unknown model parameters.

This master thesis is concern with the development of a methodology for FE model updating of structures in the frequency domain based on FRF and TR data. The ultimate objective is the creation of an efficient updating procedure, that does the adjustment of the FE model in a physically meaningful way, based on the concept of TR, and to discus the applicability of this technique when compared with the conventional method based on the FRF data.

These two methodologies were implemented and tested using experimental data obtained from two different structures, a beam and an aircraft-like structure.

The relevant goals of this work are:

- the development of a FE model updating methodology based on the FRF, making use of correlation functions;
- the development of a FE model updating methodology based on the TR functions, making use of correlation functions;

- model validation and testing of the FE model updating methodology developed for different problems, using experimental data;
- discussion of the applicability of the model updating methodology based on the TR concept in comparison with the convention FRF model updating methodology;

1.3 Outline of Thesis

The following outline of the thesis briefly summarizes the content of each chapter.

Chapter 2 addresses all the major topics and theory necessary to the work developed. The linear elasticity theory for solids in introduced and all the major assumptions made are discussed. The FE method is also presented in the theoretical point of view. In terms of mechanical of vibration analysis, the relevant topics discussed include, modal analysis, FRF and TR functions. The major equations implemented in the model updating procedures are presented in these sections. Finally, the FE model updating and optimization procedures are discussed as well as the correlation functions used in the optimisation process.

Chapter 3 is concerned with the numerical and experimental methodologies adopted in this work. The first part of this chapter gives a detailed description of the all the steps taken in the development of the updating procedure, including the explanation of the FE methodology adopted, definition of the objective functions based on the FRF and TR correlation functions and description of the optimization algorithm used in the model updating procedures. Finally a general description of the global updating procedure, using either FRF or TR experimental data is given, as well as the assumptions made in the in the creation of the FE models. The second part of this chapter addresses the experimental procedures. The experimental testing consists basically in the analysis and the extraction of predefined FRF curves of two different models. This final section includes a listing of all the equipment used in the experimental testing, and also a brief description of the experimental setup for both models, and experimental procedure in the extraction of the FRF curves.

Chapter 4 corresponds to the results section of this work. This chapter may be divided into two major sections. One relative to the analysis of a simple beam structure and another where a more complex aircraft-like model is analysed. For each of the structures considered, a preliminary analysis is performed using the same basic model, except for a few minor modifications. These preliminary models are used essentially for FE method and updating procedure verification purposes. The results obtained with these beam and aircraft models are compared with corresponding results presented in the literature. Finally, the experimental beam and aircraft models are presented. The updating results obtained based on the FRF and TR correlation functions are discussed and compared for each one of the analysed structures.

Chapter 2

Background

In this chapter a brief introduction to the linear elasticity theory for solids is presented. The principal concepts and essential equations to the work developed throughout this thesis are also presented. This includes modal analysis, frequency response and TR functions and also the definition of correlation functions, fundamental to the updating procedure developed.

In the final part of this chapter, FE model updating techniques and optimization algorithms are also discussed.

2.1 Linear Elasticity Theory for Solids

When considering small displacements and linear elastic material behavior, the underlying method to the theory of linear elasticity may be applied. This theory carries a few assumptions as presented next [9].

Practically all materials possess to a certain extent, the property of elasticity. In other words, if external forces, inducing the deformation of a structure, do not exceed a certain limit, the deformation disappears completely after removal of these forces. The relations presented in this section assume that the structures are perfectly elastic. It will also be assumed that the matter of these elastic bodies is homogeneous and regularly distributed over its volume. As a final simplifying assumption, it is considered that the elastic properties are all the same in all directions, that is, the bodies are isotropic [10].

Experience shows that solutions of the theory of linear elasticity based on the simplifying assumptions of homogeneity and isotropy can be applied in most cases with great accuracy [10].

2.1.1 Elastodynamics Equation

Elastic solids will deform as a result of applied loadings, and these deformations can be quantified by knowing the displacements of material points in the body.

In order to quantify these deformations, a simple analysis is performed defining the displacement of two generic points in a structure, referring to the undeformed and deformed solid.

Introducing the small displacements theory, a set of equations in the linearized form are obtained, which are normally referred to as the strain-displacement relations. These relations can be written in the form presented in equation (2.1).

$$\varepsilon_{ij} = \frac{1}{2}\left(\frac{\partial u_i}{\partial x_j} + \frac{\partial u_j}{\partial x_i}\right) = \frac{1}{2}(u_{i,j} + u_{j,i}) \qquad i,j = 1,2,3 \tag{2.1}$$

where x_i represents the Cartesian coordinates and u_i the displacement vector. The term $u_{i,j}$ expresses the partial derivative of the displacement u_i in respect to x_j in tensor notation, $()_{,j} = [\partial/\partial x_j]$.

External forces can be categorized into two major groups, body and surface forces. Body forces are proportional to the body's mass. Examples of these forces include gravitational, magnetic and inertial forces. On the other hand, surface forces always act on the surface and are the result of physical contact with another body [11]

Subjecting an elastic body to external loading, not only causes its deformation, but also creates an inner state of stress in the body. The stress state of the material is characterized with the stress tensor represented by the components σ_{ij}. Knowing these components σ_{ij}, it becomes possible to know the components of the stress vector, t_i, which represents the stress acting on a generic surface.

$$t_i = \sigma_{ij} n_j \tag{2.2}$$

where n_j represents the vector normal to the surface [11].

Consider a closed subdomain with volume V and involving surface S of a body in equilibrium as represented in figure 2.1. This body as a general distribution of surface stress t over its surface S and also body forces represented by f.

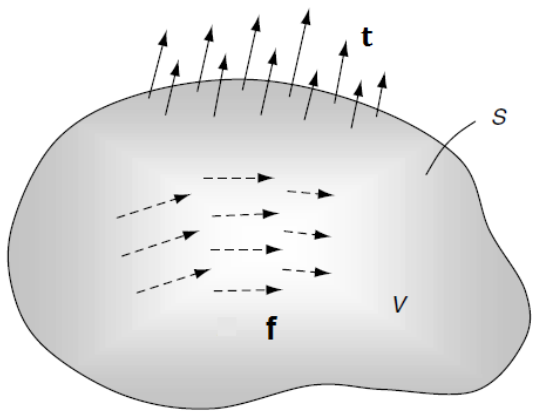

Figure 2.1: Body and surface forces acting on a generic body in equilibrium, adapted from [11]

For the equilibrium, the conservation of linear momentum implies that the forces applied on this arbitrary body are balanced. This concept can be written in index notation as:

$$\iint_S t_i \, dS + \iiint_V f_i \, dV = \iiint_V \rho \ddot{u}_i dV \tag{2.3}$$

where ρ is the density of the material and $\ddot{u}_i$ the second derivative of the displacement in respect to time.

Applying the divergence theorem (Gauss theorem) and using the relation in equation (2.2), this equilibrium can also be expressed in terms of stress:

$$\iint_S \sigma_{ji} n_j \, dS + \iiint_V f_i \, dV = \iiint_V (\sigma_{ji,j} + f_i) \, dV = \iiint_V \rho \ddot{u}_i dV \tag{2.4}$$

Considering that the region V is an arbitrary volume, the relation presented, known as the equilibrium equation, can be expressed as:

$$\sigma_{ji,j} + f_i = \rho \ddot{u}_i \tag{2.5}$$

which represents the known Cauchy's law of motion for a continuum body in equilibrium.

Taking into consideration the assumptions made of a perfectly elastic and isotropic bodies, the generalized Hooke's law for linear isotropic elastic solids can be applied, which means that the tensor of stress is linearly proportional to the tensor of strain:

$$\sigma_{ij} = E_{ijkl} \varepsilon_{kl} \tag{2.6}$$

Considering the isotropic properties of the material, with identical elastic properties in every direction, it follows that only two elastic constants are needed to describe the behavior of these materials, as shown in equation (2.7). At last, the Hooke's law relating the the tensors of stress and strain, for a elastic, homogeneous and isotropic solid assumes the following final form:

$$\sigma_{ij} = \lambda \varepsilon_{kk} \delta_{ij} + 2\mu \varepsilon_{ij} \tag{2.7}$$

where δ_{ij} represents the Kronecker delta. The elastic constant λ and μ are known as the first and second Lamé's constants, respectively. The second Lamé's constant μ, may also be represented also represented by G, and referred to as the shear modulus or modulus of rigidity. These elastic constants can also be expressed in terms of the other constants as presented in the following relations, where ν represents the Poisson coefficient:

$$\lambda = \frac{E}{(1+\nu)(1-2\nu)} \tag{2.8}$$

$$\mu = G = \frac{E}{2(1+\nu)} \tag{2.9}$$

2.1.2 Elastodynamic Response of Beam

Throughout this thesis the only type of FE that will be used is the beam element based on the Timoshenko beam model theory.

The solution of equations of vibration of the Timoshenko beam will be presented in this section. The complete demonstration on how to calculate the natural frequencies of a simply supported beam based on this theory is presented in Appendix A.

The final solution presented next follows the notation and structure as presented in the paper [12]. Considering the Timoshenko beam theory, the form of the solution to the differential equations (2.10) and (2.11) depends on the vibration frequency. The change of solution form occurs when the frequency crosses a specific value of $\omega = \sqrt{(GkA)/(\rho I)}$. Since we are only interested in a low range of frequencies,

it will only be presented the solution for the frequencies below the given limit.

The set of coupled differential equations for transverse vibration of uniform Timoshenko beam with a constant cross section are given by:

$$\frac{\partial}{\partial x}\left[kGA\left(\frac{\partial y(x,t)}{\partial x}-\Theta(x,t)\right)\right]=\rho A\frac{\partial^2 y(x,t)}{\partial t^2}-q(x,t) \tag{2.10}$$

$$kGA\left(\frac{\partial y(x,t)}{\partial x}-\Theta(x,t)\right)-\frac{\partial}{\partial x}\left(EI\frac{\partial\Theta(x,t)}{\partial x}\right)=I\rho\frac{\partial^2\Theta(x,t)}{\partial t^2} \tag{2.11}$$

where: k - Timoshenko shear coefficient depending on the cross section of the beam, G - shear modulus, A - cross sectional area, E - Young modulus, I - second moment of area, ρ - density and $q(x,t)$ the external force.

The functions that give the solution of these equations are the vibration amplitude $y(x,t)$, and the angle due to pure bending $\Theta(x,t)$.

The final solution for the equations of vibration of the Timoshenko beam element as presented in [12] uses the following notation:

$$a=\frac{\omega^2\rho}{kG};\qquad b=\frac{\rho\omega^2}{E}-c;\qquad c=\frac{GkA}{EI};\qquad d=a+b+c=\frac{\omega^2\rho I\left(1+\frac{E}{Gk}\right)}{EI} \tag{2.12}$$

$$e=ab=\frac{\omega^2\left(\omega^2\rho^2\frac{I}{Gk}\rho A\right)}{EI};\qquad \Delta=d^2-4e=\omega^4\rho^2I^2\left(1-\frac{E}{kG}\right)^2+4EI\omega^2\rho A \tag{2.13}$$

$$\lambda_1^2=\frac{-d+\sqrt{\Delta}}{2};\qquad \lambda_2^2=\frac{d+\sqrt{\Delta}}{2} \tag{2.14}$$

The nontrivial solution for this problem, after applying the necessary boundary conditions (BC), is obtained from the condition that the determinant of the matrix presented in equation (2.15) is equal to zero (see Appendix A)

$$D=\begin{bmatrix} sinh(\lambda_1 l) & sin(\lambda_2 l) \\ \lambda_1^2 sinh(\lambda_1 l) & -\lambda_2^2 sin(\lambda_2 l)\end{bmatrix} \tag{2.15}$$

$$det(D)=-(sinh(\lambda_1 l)\cdot\lambda_2^2 sin(\lambda_2 l)+\lambda_1^2 sinh(\lambda_1 l)\cdot sin(\lambda_2 l))=0 \tag{2.16}$$

where l represents the length of the beam.

The expression presented allows us to calculate the natural frequencies ($\omega = 2\pi f$) of a simply supported beam according to the Timoshenko beam theory, keeping always in mind that this result is only valid up to a frequency limit of $\omega=\sqrt{(GkA)/(\rho I)}$ (see [12]).

In Appendix B, the MATLAB code used to obtain the natural frequencies of the simply supported Timoshenko beam is provided.

2.2 The Finite Element Method

The finite element method may be defined as *"a general discretization procedure of continuum problems posed by mathematical defined statements"* [13].

The basic concept in the physical interpretation of the FE method is that the continuum is subdivided into a finite number of parts named finite elements, the behavior of which is specified by a finite number of parameters. The response of the global system is then considered to be approximated by that of the discrete model obtained by assembling all the FEs. The set of points and lines connecting each finite element is generally known as mesh and each individual point as node.

Since the majority of the problems in engineering are either extremely difficult or impossible to solve using conventional analytical methods, discretization techniques such as the FE method are applied.

The FE method discretization implies the assembling in the global mass and stiffness properties, of the elemental mass and stiffness matrices for all FEs of the mesh. Each FE forms a simple unit which can be readily analyzed, defined by a set of N_e equations corresponding to the number of Degrees of Freedom (DOF) of the respective element.

Complex geometries are usually accommodated by using a large number of FEs that consequently corresponds to a larger number of DOFs, which implies a higher set of simultaneous algebraic equations to be solved. Therefore, the number of DOFs of the FE model implies a trade-off between the required solution accuracy and the amount of computational time spent in the simulation.

Follows a brief explanation on how to obtain the general FE equation of motion for a generic solid body, starting from the equation of equilibrium as represented in section 2.1.1.

Employing the principle of virtual work, the strain-displacement relations assume the form presented in equation 2.17.

$$\delta\varepsilon_{ij} = \frac{1}{2}(\delta u_{i,j} + \delta u_{j,i}) \tag{2.17}$$

Given essential BC on the displacements u, and given natural BC, applying the residual method, considering the homogeneity of the body (constant density), the elastodynamic problem defined in equation (2.4) is reduced to the form presented in equation (2.18) [13, 14].

$$\iiint_V \delta\varepsilon_{ij}\sigma_{ij}dV = \iint_S \delta u_i t_i dS + \iiint_V \delta u_i f_i dV - \iiint_V \delta u_i \rho \ddot{u}_i dV \tag{2.18}$$

The Galerkin aproximation for the FE and for the virtual displacements is given by [15]:

$$u = \sum_\alpha N_\alpha u_\alpha \qquad \delta u = v = \sum_\beta N_\beta v_\beta \qquad \alpha, \beta = 1, 2, 3, ...NDOF \tag{2.19}$$

where N_α and N_β represent the shape functions, which is dependent on the FE used.

After some mathematical manipulation and by virtue of the property of definite integrals stating that the total be the sum of the parts [13], we obtain the following FE equation for each element of a 3D elastic body:

$$\{v\}^T\left([M]^e\{\ddot{u}\}^e + [K]^e\{u\}^e\right) = \{v\}^T\{f\}^e \tag{2.20}$$

where $[M]^e$ and $[K]^e$ represent the mass and stiffness matrices, respectively, and $\{f\}^e$ the load vector, for each element. Finally, changing the displacement notation from $\{u\}$ to $\{x\}$, the dynamic equations of motion, commonly known simply as equations of motion, for a system with no damping, can be expressed in the following form:

$$[M]\{\ddot{x}\} + [K]\{x\} = \{f\} \tag{2.21}$$

2.3 Mechanical Vibration Analysis

Essential to the analysis of vibrating structures is the ability to describe the response of a system as a function of position, $\{x(t)\}$, and time, t, given an exciting input force, $\{f(t)\}$. The interaction between the properties of mass and elasticity of a structure result in this phenomenon called "vibration" [16].

The dynamic equations of motion can be derived from force balance consideration using Newton's second law [17], or the fact that the energy content of a conservative system is constant.

Models are formally distinguished by the number of DOF of the system, N. Usually, systems of practical interest are continuous and complex in geometry (so that $N \to \infty$, being N the number of DOFs in the model). The dynamic analysis of these systems leads us to partial differential equations as functions of both space and time. Apart from the simplest geometries, obtaining the close-form solution of most structural models used in practical applications, soon becomes an impractical or even impossible exercise.

In cases where no close-form solution is feasible, discretization techniques are applied like the finite element method. The discrete modeling of these structures along with its simplifying assumptions, determine the success of the mechanical vibration analysis.

The arising necessity of validation and improving the quality of these discrete models urged the development of new techniques such as model updating.

2.3.1 Equations of Motion

The total mass and stiffness distribution of a discrete dynamic system can be used to express the balance between the interacting forces at N DOFs. The equations conferred in this section were adapted from [16].

From the dynamic equilibrium equations for a N DOFs system, the corresponding Equation of Motion (EOM) for a discrete model and assuming viscous damping, is conveniently written in a matrix notation as:

$$[M]\{\ddot{x}(t)\} + [C]\{\dot{x}(t)\} + [K]\{x(t)\} = \{f(t)\} \tag{2.22}$$

Equation (2.22) is composed by a set of N linear ordinary differential equations stating that the internal stiffness, damping, and inertial related forces are in equilibrium with the externally applied forces $\{f(t)\}$.

Analyzing the system for its harmonic response properties by assuming steady-state conditions, so that we have $\{x(t)\} = \{X\}\,\mathrm{e}^{\imath\omega t}$ when $\{f(t)\} = \{F\}\,\mathrm{e}^{\imath\omega t}$, equation (2.22) assumes the form presented in equation (2.23).

$$(-\omega^2[M] + \imath\omega[C] + [K])\{X\} = \{F\} \tag{2.23}$$

$$([Z] + \imath\omega[C])\{X\} = \{F\} \tag{2.24}$$

where $[Z]$ is the undamped dynamic stiffness matrix. The corresponding response model is given by $\{X\} = [H]\{F\}$, with:

$$[H] = ([Z] + \imath\omega[C])^{-1} \tag{2.25}$$

where $[H]$ corresponds to the receptance FRF matrix, defined as the ratio of displacement to force.

2.3.2 Modal Analysis

A steady state forced response analysis can be performed directly from equation (2.23). On the other hand, one can use modal parameters to calculate the FRFs.

For an undamped system ($[C] = [0]$), the modal parameters refer to a set of eigenvalues and eigenvectors corresponding to the natural frequencies and mode shapes of the system, respectively. If there is no external excitation, i.e. $\{f(t)\} = \{0\}$, the structure is capable of vibrating naturally, therefore these eigenvalues and eigenvectors are referred to as the “natural” or “normal” modes of the structure [18]. Each eigenvector constitutes a relative set of modal displacements corresponding to its natural frequency.

With no external forces applied and for an undamped system, the vibrating response will not degenerate with time and the harmonic trial response assumes the form $\{x(t)\} = \{X\}\,\mathrm{e}^{\imath\omega t}$. Therefore, the problem of obtaining the modal parameters is reduced to solving:

$$(-\omega^2[M] + [K])\{X\} = \{0\} \tag{2.26}$$

If the mode shapes (eigenvectors) and the corresponding natural frequencies are designated by $\{\psi\}_r$ and ω_r, the previous equation assumes the form:

$$(-\omega_r^2[M] + [K])\{\psi\}_r = \{0\} \quad \text{for} \quad r = 1, 2, 3, ..., N \tag{2.27}$$

The eigenvalues of the system are defined as $\lambda_r = \omega_r^2$. Equation (2.27) is satisfied exactly by N modes for a system of N DOFs.

The matrices $\begin{bmatrix} \ddots & & \\ & \lambda_r & \\ & & \ddots \end{bmatrix}$ and $\begin{bmatrix} & & \\ & \Psi & \\ & & \end{bmatrix}$ are respectively designated by the diagonal eigenvalue matrix and the eigenvector or modal matrix, in which the eigenvectors are organized by columns.

The orthogonality property of the mode shapes allows the simplifications of the analysis of the system to a great extend.

$$\left[\ \Psi\ \right]^T \left[\ M\ \right] \left[\ \Psi\ \right] \quad = \left[\ m_r\ \right] \tag{2.28}$$

$$\left[\ \Psi\ \right]^T \left[\ K\ \right] \left[\ \Psi\ \right] \quad = \left[\ k_r\ \right] \tag{2.29}$$

where $\left[\ m_r\ \right]$ and $\left[\ k_r\ \right]$ are the effective modal mass and stiffness diagonal matrices, respectively.

In order to establish a consistent scaling of the mode-shapes, the eigenvectors are often mass-normalized:

$$\{\phi\}_r = \frac{\{\psi\}_r}{\sqrt{\{\psi\}_r^T [M] \{\psi\}_r}} \tag{2.30}$$

where ϕ^r is the rth mass-normalized mode-shape vector. Taking into account the orthogonality properties, the following conditions arise:

$$\left[\ \Phi\ \right]^T \left[\ M\ \right] \left[\ \Phi\ \right] = \left[\ I\ \right], \tag{2.31}$$

$$\left[\ \Phi\ \right]^T \left[\ K\ \right] \left[\ \Phi\ \right] = \left[\ \lambda_r\ \right], \tag{2.32}$$

$$\left[\ \Phi\ \right]^T \left[\ C\ \right] \left[\ \Phi\ \right] = \left[\ (\ 2\,\xi_r\,\omega_r\ )\ \right] \tag{2.33}$$

where ξ_r is the rth modal viscous damping ratio.

Damping is the mechanism by which the system's kinetic energy is gradually dissipated, e.g. converted into heat or sound. Rayleigh or proportional damping is a form of viscous damping that is proportional to the linear combination of the mass and stiffness.

$$\left[\ C\ \right] = \alpha \left[\ M\ \right] + \beta \left[\ K\ \right] \tag{2.34}$$

where parameters α and β represent the mass and stiffness proportional damping coefficients respectively and they can be determined experimentally. From the Rayleigh damping equation follows that [19]:

$$\xi_r = \frac{\alpha}{2\,\omega_r} + \frac{\beta\,\omega_r}{2} \tag{2.35}$$

$$2\,\xi_r\,\omega_r = \alpha + \beta\,\omega_r^2 \tag{2.36}$$

2.3.3 Frequency Response Functions

Considering an harmonic excitation force, $\{f(t)\} = \{F\}\,\mathrm{e}^{\imath\omega t}$, and the consequent harmonic response, $\{x(t)\} = \{X\}\,\mathrm{e}^{\imath\omega t}$, on a linear structure assuming viscous damping, the receptance FRF matrix is defined as presented in equation (2.38).

$$[X] = [H]\{F\} \tag{2.37}$$

$$\left[\, H(\omega) \,\right] = \left(-\omega^2 \left[\, M \,\right] + \imath\, \omega \left[\, C \,\right] + \left[\, K \,\right] \right)^{-1} \tag{2.38}$$

Considering the modal orthogonality properties and after some algebraic manipulation [18], the FRF receptance matrix can be expressed as:

$$\left[\, H(\omega) \,\right] = \left[\, \Phi \,\right] \left[\diagdown \left(\omega_r^2 - \omega^2 + \imath\, \omega\, 2\, \xi_r\, \omega_r \right) \right]^{-1} \left[\, \Phi \,\right]^T \tag{2.39}$$

Considering the Rayleigh damping relationship, the FRF matrix can also be defined as:

$$\left[\, H(\omega) \,\right] = \left[\, \Phi \,\right] \left[\diagdown \left(\omega_r^2 - \omega^2 + \imath\, \omega\, (\alpha + \beta\, \omega_r^2) \right) \right]^{-1} \left[\, \Phi \,\right]^T \tag{2.40}$$

Equation (2.40) reduces the computational cost appreciably, considering that it is only necessary to compute the inverse of a diagonal matrix instead of using equation (2.38) directly.

In cases were only individual FRF are required, the above expression can be further reduced to the following summation [16]:

$$H_{ij}(\omega) = \sum_{r=1}^{N} \frac{\phi_{ir}\phi_{jr}}{\omega_r^2 - \omega^2 + \imath\omega(\alpha + \beta\omega_r^2)} \tag{2.41}$$

where all N modes are included, and i and j correspond to the response and excitation locations respectively in the eigenvector of the rth mode.

It has be proven that the FRFs can be computed from a limited number of modes with sufficient accuracy even for response analysis over a wide range frequency range. Therefore, equation (2.41) becomes:

$$H_{ij}(\omega) \approx \sum_{r=1}^{m} \frac{\phi_{ir}\phi_{jr}}{\omega_r^2 - \omega^2 + \imath\omega(\alpha + \beta\omega_r^2)} \tag{2.42}$$

where m can be rather small compared with the total number of modes, $m \ll N$, reducing the computational cost considerably.

The validity of this approximation arises from the fact that higher modes participate very weakly in lower frequency regions. Since the work developed in this thesis only concerns a relatively low range of frequency, this approximation will be adopted, always considering the required accuracy for each simulation.

Considering the following velocity and acceleration relationships

$$\{v(t)\} = \{\dot{x}(t)\} = \imath\omega\{X\}\,\mathrm{e}^{\imath\omega t} \qquad \{a(t)\} = \{\ddot{x}(t)\} = -\omega^2\{X\}\,\mathrm{e}^{\imath\omega t} \tag{2.43}$$

respectively, the alternative forms of FRF matrices, in terms of velocity and acceleration, are presented:

$$Mobility\ FRF:\ [Y] = \imath\omega[H] \tag{2.44}$$

$$Accelarance\ FRF:\ [A] = -\omega^2[H] \tag{2.45}$$

The experimental FRF values correspond to the accelerance FRF values. In order to compare these results with the numerical ones, we will only use these accelerance FRFs, which will receive the notation of $[H]$ instead of $[A]$. The unis of these FRFs are $(m/s^2)/N$.

2.3.4 Transmissibility Functions

The concept of TR for MDOF systems has been developed and applied for many years [20]. The various ways in which the TR concept can be defined and applied, opens a wide range of research possibilities for improvements in fields such as model updating [21].

In this section the concepts of force TR and displacement TR in MDOF systems will be revisited as presented in the papers [22, 23].

Displacement Transmissibility

A set of coordinates for a generic MODF system is defined as in figure 2.2: (i) **K** the set of coordinated where the responses are known; (ii) **U** is defined as the set of coordinates where the responses are unknown; (iii) **A** the coordinates where the forces F are applied and (iv) **C** represents all the other coordinates.

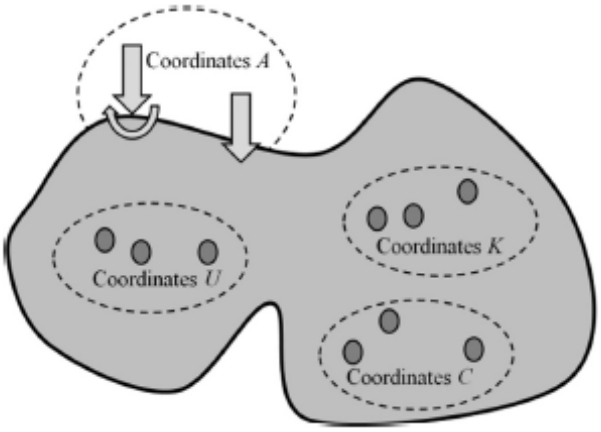

Figure 2.2: MDOF system illustration with the set of coordinates K, U, A and C [22]

The relation between the responses and the external excitation forces, only when $F_A \neq 0$ can be expressed as:

$$\begin{Bmatrix} X_A \\ X_U \\ X_K \\ X_C \end{Bmatrix} = \begin{bmatrix} H_{AA} \\ H_{UA} \\ H_{KA} \\ H_{CA} \end{bmatrix} \cdot \{F_A\} \tag{2.46}$$

Assuming an harmonic excitation force applied at coordinates A and steady-state conditions, the relation between the applied forces and the displacements at the coordinates U and K can be expressed as:

$$\{X_U\} = [H_{UA}]\{F_A\} \tag{2.47}$$

$$\{X_K\} = [H_{KA}]\{F_A\} \tag{2.48}$$

Eliminating $\{F_A\}$ between 2.47 and 2.48, the transmissibility relating both sets of displacements can be expressed as:

$$\{X_U\} = [T_{UK}^{(d)}]\{X_K\} \tag{2.49}$$

$$[T_{UK}^{(d)}] = [H_{UA}][H_{KA}]^{+} \tag{2.50}$$

where the upper index $^{(d)}$ stands for displacement transmissibility and $[H_{KA}]^{+}$ represents the pseudo-inverse matrix of $[H_{KA}]$ [24].

Force Transmissibility

First of all, it is necessary to define a set of coordinates for a generic MDOF system as in figure 2.3: (i) **K** is the subset of coordinates where the external forces are applied; (ii) **U** coordinates where the reaction forces appear due to displacement constraints; (iii) **C** constitutes all the other coordinates.

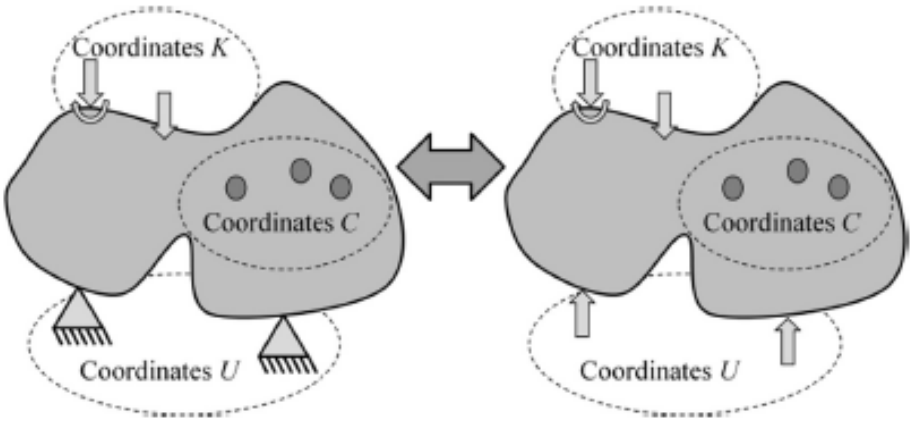

Figure 2.3: MDOF system illustration with the set of coordinates K, U and C [22]

The receptance FRF matrix in steady state conditions, relates the dynamic displacement amplitudes $\{X\}$ with the external force amplitudes $\{F\}$. Introducing the set of coordinates K, U and C, the relationship can be expressed as:

$$\begin{Bmatrix} X_K \\ X_U \\ X_C \end{Bmatrix} = \begin{bmatrix} H_{KK} & H_{KU} \\ H_{UK} & H_{UU} \\ H_{CK} & H_{CU} \end{bmatrix} \cdot \begin{Bmatrix} F_K \\ F_U \end{Bmatrix} \tag{2.51}$$

Assuming the responses at the reactions coordinates U as zero, i.e. $\{X_U\} = \{0\}$, it follows that:

$$[H_{UK}]\{F_K\} + [H_{UU}]\{F_U\} = \{0\} \tag{2.52}$$

$$\{F_U\} = -[H_{UU}]^{-1}[H_{UK}]\{F_K\} \tag{2.53}$$

Therefore, the force transmissibility between set of coordinates U and K can be expressed as:

$$\{F_U\} = [T_{UK}^{(f)}]\,\{F_K\} \tag{2.54}$$

$$[T_{UK}^{(f)}] = -[H_{UU}]^{-1}\,[H_{UK}] \tag{2.55}$$

where the upper index $^{(f)}$ stands for force transmissibility.

Throughout this thesis, only the force TR is used in order to simplify the presentation of the final results. The TR functions will be simply represented by T.

2.4 Finite Element Model Updating

Finite element model updating is an inverse problem used to correct uncertain modeling parameters leading to a better prediction of the dynamic behavior of structures [25, 26].

To understand the lack of correlation between the predictions and the experimental responses, it is necessary to consider the probable causes of such inaccuracy. Two forms of modeling errors which may lead to this inaccuracy are: (i) model parameter errors, which include the uncertainty on the exact parameter values and the inappropriate application of the BC; (ii) model order errors, which result from inappropriate discretization of complex systems [1].

While creating a FE model, it is common to make certain simplifying assumptions. Ultimately the analyst establishes the model, which according to his engineering judgment will produce adequate and accurate results. In [18] a study is presented comparing the FE results produced by 12 different engineers working independently, showing that some results differ considerably from others.

Typically, design optimization is preceded of model updating in order to establish a numerical model that predicts more accurately the dynamic behavior of a structure given certain changes. While parameter selection in design optimization is mainly constrained by manufacturing requirements, choosing the correct updating parameters is the key factor for a successful model updating, requiring deep knowledge about the FE model assumptions made and possible sources of model errors [1].

Most finite element dynamic model updating methods use resonance frequencies and mode shapes. Despite having proven their value, these modal-based model updating methods are extremely dependent on the quality of the modal parameters extraction. In [27] a model updating technique is proposed, which uses resonance and anti-resonance frequencies for better FRF matching.

In 1995, the state-of-the-art in model updating was still focused on the use of modal-based techniques since they were more robust and better understood for practical application than other FRF-based model updating methods. The limitations of modal-based updating and more stringent design requirements, motivated further research in the subject of FRF-based model updating techniques [16].

The TR-based model updating methods is still lacking research when compared with other techniques. In the paper [3], a new technique to update the FE model from the output-only TR measurements is presented, as well as its comparative advantages.

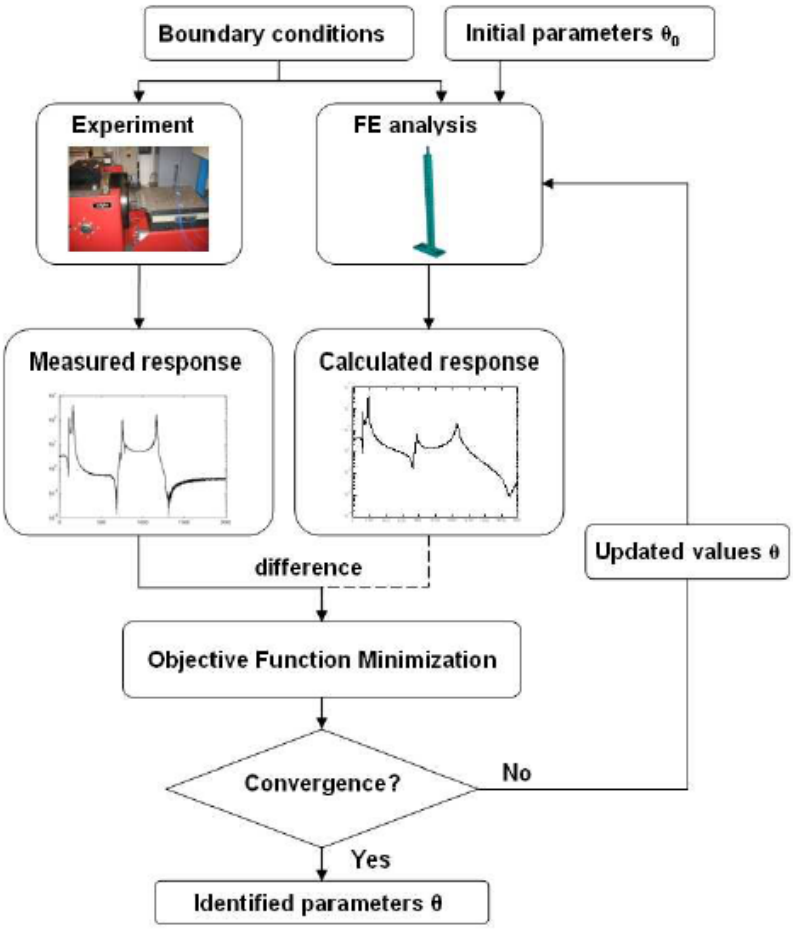

Figure 2.4: Flowchart of a generic FE model updating problem [25]

An important objective of this master thesis is to research and conclude about the applicability of updating FE models based on the TR functions when comparing with conventional FE model updating methods such as FRF-based updating techniques.

At first, the numerical modal data is extracted from the FE model using initial estimates for the unknown and updating parameters. The experimental data is obtained from structural testing. In an iterative process, the selected updating parameters are adjusted in order to minimize the differences between the experimental and numerical data. In terms of displacement BC, it is usual in experimental studies to analyse the structure suspend using elastic strings to approach the free state. The general procedure of FE model updating is shown in Figure 2.4.

2.5 Numerical Optimization of FE Models

Finite element model optimization offer the possibility of identifying unknown model parameters by iteratively reducing the discrepancy between calculated and the desired responses. In FE model updating, the optimization procedure targets the minimization of an objective function for which the input data

is given by the target responses of the system.

The boundaries or constraints applied to the optimization model parameters can be based on the physical admissible bounds but they can also be implemented in order to increase optimization stability therefore avoiding convergence problems.

Most conventional optimization procedures consist mainly on two iterative processes [25]:

1. FE model analysis and response calculation based on design parameter values given as input for the numerical FE model,

2. Objective function minimization and generation of new design parameter values

The flowchart present in Figure 2.5 describes a general optimization approach and it can be found in multiple publications in which the optimization problem is addressed such as [25, 28].

Usually the optimization procedures are performed using a combination of commercially available FE software (e.g. Siemens NX, Abaqus, ANSYS) and additional user-written routines (e.g. MATLAB) for optimizing the FE model by minimization of an objective function.

There are several optimization algorithms available and implemented in the MATLAB optimization Toolbox itself [29].

The first step in the optimization procedure consists in performing a FE analysis and calculating the responses of the initial FE model with initial parameter estimates. Next, this FE data is used as input in the optimization routine (implemented in MATLAB), which generates new design parameter values after calculating the value of a pre-defined objective function. Then, the new parameter values are used to perform a new FE analysis and this process is repeated iteratively until the defined convergence criteria is achieved.

Parameter selection is the key factor for the success of FE model updating. If the selected parameters do not correspond to the real source and location of the error, the parameter values may lose their physical meaning after updating. In such cases, the updated FE model may be capable of reproducing the test data, but may not be of further use to predict the system behavior beyond the frequency range used in the updating procedure or predict the effects and responses of structural modifications.

The optimization procedures here discussed are based on the minimization of a pre-defined objective function. The selection of the appropriate objective function is also one of the key aspects of model updating. For example, in [2] the objective function is based on the correlation between the experimental and analytical FRFs while in [30] the objective function used consists in an ordinary least squares problem defined as a sum of the squared differences between measured target eigenfrequencies and the FE model numerical eigenfrequencies.

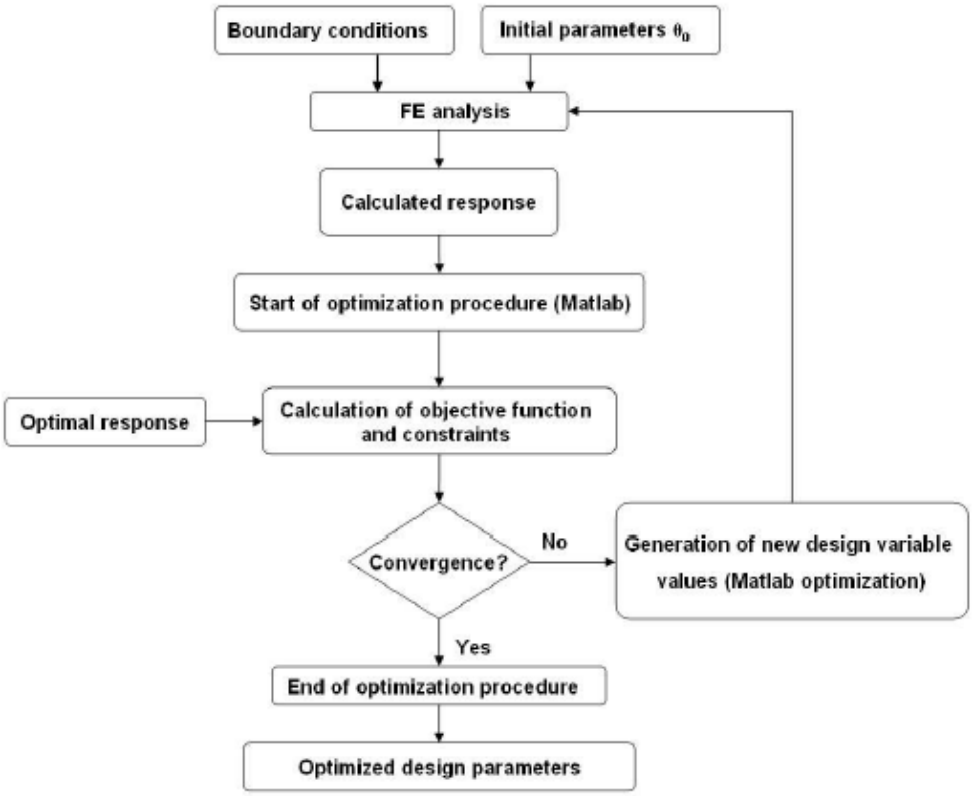

Figure 2.5: Flowchart of a conventional optimization procedure [25]

Optimization algorithms can be classified according to their convergence type into global optimization methods and local optimization methods. Deciding which optimization method to apply ultimately represents a trade-off between the accuracy of the solution and the time it will take to reach this solution.

Local optimization algorithms are very popular as they have proven to be effective and to have a fast convergence. However, they do not guarantee to find the global minimum since they can be trapped in a local minimum.

On the other hand, global optimization algorithms are more likely to find the global minimum. These methods are more robust as the choice of starting point has little influence on the final result. The main disadvantage of such algorithms is the higher number of function evaluations required.

Therefore, the efficiency of the applied optimization algorithm in terms of computational time and accuracy of the results is the major aspect to consider while deciding which algorith to use.

In the next chapter a more detailed explanation is presented on how this optimization was implemented.

2.6 Validation and Correlation Functions

Finite element analysis became an important numerical analysis tool and often plays an integral part in the design cycle [16]. It is considered good practice to validate the numerical FE model by comparing a number of predicted dynamic responses with the correspondent measurements in order to conclude

about the accuracy of the FE model. A popular way of validation is correlating the modal parameters extracted experimentally with the equivalent modal parameters from the numerical FE model.

For many years the validation of analytical model was performed using modal-based correlation techniques. In [31], Allemang and Brown proposed the very popular correlation parameters "Modal Assurance Criterion" (MAC). Values of MAC close to unity indicate a good correlation between the experimental mode shape $\{\psi_X\}_i$, and the predicted eigenvector $\{\psi_A\}_j$.

$$MAC = \frac{\left|\{\psi_X\}_i^H \{\psi_A\}_j\right|^2}{\left(\{\psi_A\}_j^H \{\psi_A\}_j\right)\left(\{\psi_X\}_i^H \{\psi_X\}_i\right)} \tag{2.56}$$

where $\{\}^H$ represents the complex conjugate (Hermitian) transpose of the column vector.

However, it is known that this correlation coefficient is incapable of differentiating between systematic errors and local discrepancies.

With the developments of the first FRF-based model updating techniques, it was common to visually check the level of correlation between the experimental and analytical FRF, overlaying the experimental data with the analytical corresponding data. Also, numerical measures have been developed to quantify the level of correlation, such as the Frequency Response Assurance Criterion (FRAC) proposed in [32].

In [2] a model updating technique is proposed using two different correlation functions: Cross Signature Assurance Criterion (CSAC) and the Cross Signature Scale Factor (CSF). Together, these two correlation functions are referred to as the Cross Signature Correlation (CSC) functions.

The correlation function CSAC was initially defined as a measurement of correlation between FRFs equivalent to the Modal Assurance Criterion (MAC), adapted to the frequency domain. The level of correlation for any measured frequency point, ω_k (with $k = 1, 2, ..N_f$, being N_f the number of measured frequency points), is evaluated as presented in equation 2.57

$$CSAC(\omega_k) = \frac{\left|\{H_X(\omega_k)\}^H \{H_A(\omega_k)\}\right|^2}{\left(\{H_X(\omega_k)\}^H \{H_X(\omega_k)\}\right)\left(\{H_A(\omega_k)\}^H \{H_A(\omega_k)\}\right)} \tag{2.57}$$

where $\{H_X(\omega_k)\}$ and $\{H_A(\omega_k)\}$ are respectively the measured and predicted response column vectors at matching excitation and response locations.

It can be seen that CSAC returns a value between zero and unity, indicating perfect correlation if $CSAC(\omega_k) = 1$ and no correlation if $CSAC(\omega_k) = 0$.

Similar to the MAC, $CSAC(\omega_k)$ is unable to detect scaling errors, as it is only sensitive to discrepancies in the overall deflection shape of the structure.

The lack of sensibility to scaling of this *shape correlation* measure, does not allow the identification of identical FRFs. This limitation becomes even more dramatic if only one measure and the corresponding prediction are correlated. In this case the column vectors are reduced to scalars and $\{H_A(\omega_k)\} = c \cdot \{H_X(\omega_k)\}$ is always verified (with constant c possibly complex), leading to $CSAC(\omega_k) = 1$ across the full spectrum of frequencies for uncorrelated FRFs [16, 33].

To overcome his problem and to completely characterize the correlation between FRFs, it is necessary to introduce a second correlation function capable of evaluating the discrepancies between amplitudes. This function referred as the Cross Signature Scale Factor (CSF) can be expressed as:

$$CSF(\omega_k) = \frac{2\left|\{H_X(\omega_k)\}^H \{H_A(\omega_k)\}\right|}{\{H_X(\omega_k)\}^H \{H_X(\omega_k)\} + \{H_A(\omega_k)\}^H \{H_A(\omega_k)\}} \tag{2.58}$$

The values of this *amplitude correlation* measure also range between zero and unity, being $CSF(\omega_k) = 1$ for a perfect correlation and $CSF(\omega_k) = 0$ in the case of no correlation. This correlation measure is more stringent and only becomes unity if $\{H_A(\omega_k)\} = \{H_X(\omega_k)\}$, i.e. all elements of the response vector must be identical in both amplitude and phase, even if only one measurement is considered.

2.7 Present Contributions

This section is concerned with the main contributions of the work developed, namely the adaptation of the correlation functions using the TR functions to the model updating problem.

Analogously to the definition of the Cross Signature Correlation functions presented in section 2.6, these functions were also defined to quantify the shape and amplitude discrepancies between the TR functions, obtained both experimentally and numerically. The correlation functions $CSAC(\omega_r)$ and $CSF(\omega_r)$ as presented in equations (2.59) and (2.60), respectively.

$$CSAC(\omega_k) = \frac{\left|\{T_X(\omega_k)\}^H \{T_A(\omega_k)\}\right|^2}{\left(\{T_X(\omega_k)\}^H \{T_X(\omega_k)\}\right)\left(\{T_A(\omega_k)\}^H \{T_A(\omega_k)\}\right)} \tag{2.59}$$

$$CSF(\omega_k) = \frac{2\left|\{T_X(\omega_k)\}^H \{T_A(\omega_k)\}\right|}{\{T_X(\omega_k)\}^H \{T_X(\omega_k)\} + \{T_A(\omega_k)\}^H \{T_A(\omega_k)\}} \tag{2.60}$$

where $\{T_X(\omega_k)\}$ and $\{T_A(\omega_k)\}$ are respectively the corresponding measured and predicted TR function vectors for the discretization of the frequency range.

Chapter 3

Numerical and Experimental Methodologies

In the following sections a detailed description of the developed numerical updating methodologies and experimental procedures are presented.

Section 3.1 describes the necessary steps towards the implementation of the model updating routines, including optimization and objective function definition as well as general overview of the updating procedure.

In terms of experimental methodologies presented in section 3.2, a brief description of the equipment used and its relevant characteristics are presented, along with the experimental procedures as well as the experimental setup schemes corresponding to both experimental structures used in is work.

3.1 Model Updating and Optimization Methodology

Model updating techniques are often described as ”iterative methods”. These methods work together with a parametrized model, in this case a FE model, and introduce changes to a pre-defined number of design parameters on an elemental basis.

In the next subsections, the updating methodology developed for this work is explained, giving a global perspective on how the updating procedure works.

3.1.1 Objective Function

An iterative model updating procedure consists in the minimization of what is referred to as the objective function. These functions, also known as ”error functions”, quantify the discrepancies between the experimental and numerical model.

In this work, two different but similar objective functions are defined. One based on the FRF correlation functions and other based on the same correlation functions applied to the TR functions.

Considering that the FRF or TR amplitude values are obtained for a frequency increment of f_{inc},

for a generic frequency range of $0\,Hz$ to f_{range}, the total number of frequency points used in obtaining these values are defined as $N_f = f_{range} \times f_{inc}$. Since the correlation functions are obtained for each frequency value of either FRF or TR curves, the total number of points for these correlation functions is also N_f.

The general expression for the objective function used in both updating procedures, regardless of appying it to the FRF or TR data is presented in equation 3.1.

$$\Delta e = N_f - \sum_{k=1}^{N_f} \left(\frac{CSAC(\omega_k) + CSF(\omega_k)}{2} \right) \tag{3.1}$$

Note that perfect correlation requires that both correlation functions assume the value 1 throughout the frequency range considered (all frequency points N_f). This means that the summation of the average between the two correlation functions for all N_f, would return the exact value of N_f, and consequently, the "error function" would return 0. On the other hand, for lower values of either correlation function, the objective function value also increases.

3.1.2 Linking MATLAB to ANSYS

The numerical models created throughout this work as well as all the necessary numerical analysis, were done using the FE method commercial code developed by ANSYS APDL [34]. Since the iterative model updating routine was done using MATLAB and all the modal analysis were done using ANSYS APDL, the problem of connecting the two programs emerged.

The files available in the MathWoks [35], were adapted in order to enable this communication. The MATLAB files made available with the extension '.cc' were compiled originating the "executables" *keyInject_setFocus.mexw64*, *keyInject_sendKey.mexw64* and *textInject.mexw64*. Then, for each APDL command to be sent from MATLAB to ANSYS, the function *Write2ANSYS.m* is called with the APDL command as the input and the function of the three "executables" is to set focus on the ANSYS command window, copy the command text and finally press enter. Figure 3.1 presents the MATLAB function *Write2ANSYS.m* in detail.

Write2ANSYS.m

```
function Write2ANSYS( commands )

windowsss='ANSYS Command Window';

%sets focus on ANSYS command window
keyInject_setFocus(windowsss);

%copies text to ANSYS command window
textInject(windowsss,1,1,sprintf(commands));

%press enter
keyInject_sendKey(windowsss,13,0);

end
```

Figure 3.1: MATLAB function *Write2ANSYS.m*

Figure 3.2 presented below, illustrates how the connection between the two programs was performed. Both programs have to be open, with the ANSYS command window as presented below.

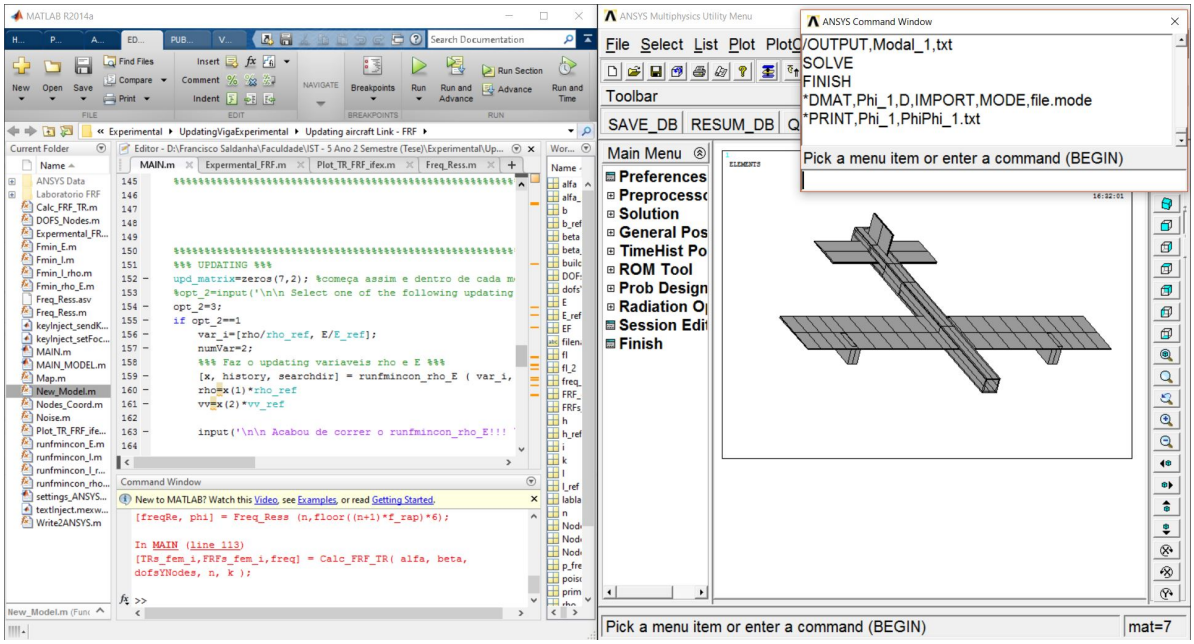

Figure 3.2: Connection between ANSYS and MATLAB

A simple way of managing this interaction is for example described in [36]. In that work, the FE analysis is done be executing an ASCII script written in ANSYS programming language APDL. This script is executed in ANSYS batch mode, which starts and exits the FE analysis software for each necessary analysis. In terms of time spent in the optimization process, it is concluded that if ANSYS could be kept running between each iteration, it would save a considerable amount of time.

In this work, the interaction between ANSYS and MATLAB is done differently. The FE analysis program ANSYS is kept running throughout the entire optimization process, by writing the ANSYS APDL commands directly in the *ANSYS Command Window* as explained above. This constitutes a great advantage in terms of saving time in the optimization process.

The fact that the FE analysis is done in ANSYS and the optimization routine is implemented in MATLAB, also constitutes an advantage since it allows for the optimization of more complex structures, without loosing the capability of complex analysis, since this capacity is entirely given by ANSYS which is specialised tool in FE analysis.

3.1.3 Optimization Routine

The model updating procedure consists mainly in the optimization of a pre-defined non-linear objective function, as described in section 3.1.1, for a defined number of varying parameters.

As discussed in section 2.5, there are different optimization algorithms according to their convergence type, global and local optimization algorithms.

In this work, we will be using a global optimization algorithm available in the MATLAB optimization Toolbox [29], known as *patternsearch*.

A few input parameters are required by this optimization function. The first one is obviously the objective function to be minimized. Depending on the number of optimization variables, two vectors have to be provided with the lower and upper BC applied to the each one of the optimization variables.

Although this is a global optimization algorithm, and therefore the starting point of the optimization variables has little influence on the final result, these values are also an input for the *patternsearch* optimization function and will be referred to as the initial updating parameter values.

In conclusion, the optimization routine consists in running the objective function iteratively using different values for the optimization variables in each iteration, until the required convergence is achieved.

There are a few additional input options for this function in terms of for example, defining more stringent convergence and stop criteria. These options were set to its default value.

3.1.4 Updating Procedure

The first step in the updating procedure is the creation of the FE model with the necessary BC, using an initial set of modeling parameter values. Then, the FE model is tested in order to obtain the numerical data necessary while the experimental data is obtained from structural testing. Afterwards, in the iterative optimization process, a set of pre-defined model parameters are adjusted in order to minimize the differences between the numerical and experimental data. Finally, given that the converge requirements are satisfied, the iterative optimization process stops and the final updated parameters are obtained.

As mentioned before, the numerical and experimental data used in the the updating problems of this work are the FRF and TR data. Follows a brief description of the the updating process as implemented in the problems considered in this work.

Considering a particular updating problem, the updating procedure begins in MATLAB with the generation of the the initial FE model in ANSYS. Then, the selected numerical data is extracted from the initial model.

A modal analysis is performed in ANSYS in order to obtain the eigenfrequencies as well as the mass-normalized mode shapes of the system. These modal data is therefore used to calculate the FRF curves using the equation 2.42.

After obtaining the numerical data and having available the corresponding experimental data, the optimization process begins. In each iteration performed, the selected updating parameters are slightly modified in the FE model, the modal data is once again extracted performing a modal analysis in ANSYS, and the value of the objective function in calculated using the numerical and experimental FRF or TR data. When the convergence criteria is met the iterative process stops and the final updating parameters values are obtained.

The updating procedure developed for each problem, having defined the values of the initial model parameters as well as the updating parameters and its optimization BC, runs without interruptions from start to end, ultimately giving us the final updated parameter values corresponding to the updated model.

It will be assumed no damping for all the FE models created throughout this thesis. This will lead to

some amplitude discrepancies, between the numerical and experimental data, especially noted close to the resonance frequency peaks.

All the FE models generated throughout this thesis use simple beam elements based on the Timoshenko theory as described in section 2.1.2. The beam element that will be used in ANSYS corresponding to the Timoshenko beam theory, is the *Beam188* element.

3.2 Experimental Methodology

In this section a brief explanation of the experimental tests will be provided, including a listing of the equipment used and the experimental procedure adopted for the testing of each one of the experimental models.

The sole objective of the experimental testing, was to obtain the necessary FRF amplitude values, for model updating purposes, extracting these values for a specified number of frequency points within a particular frequency range of interest.

3.2.1 Equipment Listing

The list of the equipment used in the experimental testing along with the corresponding model are presented in the table 3.1.

Type of Equipment	**Model**
Impact Hammer	PCB 208C01
Piezoelectric Accelerometer	Bruel & Kjaer 4508 B
Piezoelectric Force Transducer	Bruel & Kjaer Type 8200
Data Acquisition Hardware for PULSE	Bruel & KjaerType 3160-A-042

Table 3.1: List of major equipment used in the experimental testing

For the impact hammer, there were three different types of tips, steel plastic and rubber. The testing was done using only the plastic tip. Attached to the hammer was the force transducer in order to measure the excitation force applied to the structure during the experimental testing.

The piezoelectric accelerometer was used to measure the response of the structure in terms of acceleration. This response transducer is unidirectional, meaning it can only measure the acceleration response in one direction, and the signal output is done through a coaxial cable.

Another equipment used in the experimental testing is a computer with the Bruel & Kjaer software PULSE installed.

3.2.2 Experimental Procedure

The experimental setup scheme for a generic structure is presented in figure 3.3. The impact of the hammer in specimen triggers a signal in the force transducer which measures this input signal corre-

sponding to the excitation force applied to the structure. Consequently, the accelerometer assembled to the structure, measures the response of the structure, resulting from this impact, in terms of acceleration (output signal). These signals are collected in the data acquisition hardware unit, and analysed using the PULSE software.

In terms of software configuration, the frequency range considered in all tests performed was $0\,Hz$ to $400\,Hz$ with a frequency interval increment of $0.5\,Hz$, which means that 800 frequency points were considered for each frequency response curve extracted.

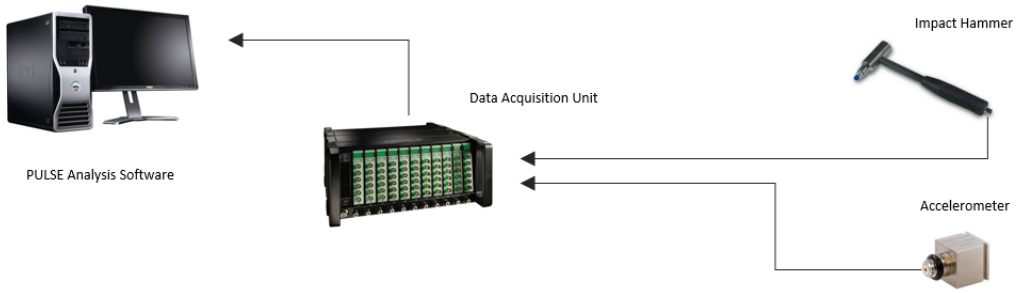

Figure 3.3: Generic scheme of the experimental setup

In order to obtain one single frequency response curve, five different impacts had to be performed, that is, five different measurements, meaning that the final response values obtained for each frequency point correspond to the average of these five measurements.

The results obtained for each curve extracted included, the frequency response values for both amplitude and phase, and the coherence between the five different measurements performed.

As it will be discussed in the results section of this work, the correlation curve obtained for each one of the extracted FRFs, are a good indication of the quality of the values obtained, since it indicates the consistency of the values obtained for each frequency values.

Two different structures were tested. A simple beam and a aircraft like structure.

The beam was suspended by two elastic strings from a fixed support. Figure 3.4 illustrates the experimental setup for the beam experimental tests. The exact location of the excitation and measuring locations will be presented in the results section 4.2, in which the corresponding FE model is introduced as well as the beam measured length, cross section width and height. For the three measurement locations, bees-wax was used to fix the accelerometers to the structure in the desired direction of measurement.

Figure 3.4: Beam experimental setup scheme

The experimental setup of the aircraft for the experimental testing is presented in figure 3.5. The aircraft was also suspended by two elastic strings from a fixed structure using two elastic strings. The two holes located in the nose part of the aircraft were used to attach both extremities of the strings.

Figure 3.5: Beam experimental setup scheme

As stated before, the results of the amplitude of response as well as the correlation curves, were obtained from the software PULSE, in the form of ".txt" files. For each updating simulation, these values were extracted using MATLAB.

For a more detailed discussion on experimental procedures of this type, see e.g. [37] and [14].

Chapter 4

Results and Discussion

This chapter is divided into two major topics. One concerning verifications on simple examples (analysis of a beam structure) and another where a more complex structure, even if simplified, aircraft-like structure is analysed.

As described in the objectives sections, one major concern of this work is to analyse and verify how the developed model updating methodology behaves when applied to different updating problems.

For each one of the structures considered, a preliminary analysis is performed using the same generic structure but with a few minor modifications. These preliminary results serve as a means of comparison with the final numerical models, in terms of verification of the FE method and the updating procedure, by comparing the results obtained, with the results of similar models already developed in the literature.

Finally, the two updating methodologies based on the FRF and TR correlation functions, described in chapter 3, are applied both to the beam and aircraft-like structures.

4.1 Simply Supported Beam

In this first section, the results in terms of obtaining the transmissibility curves are presented as in the paper [22], using the same basic model, a simply supported beam. Figure 4.1 shows the beam model as presented in the paper without the BC:

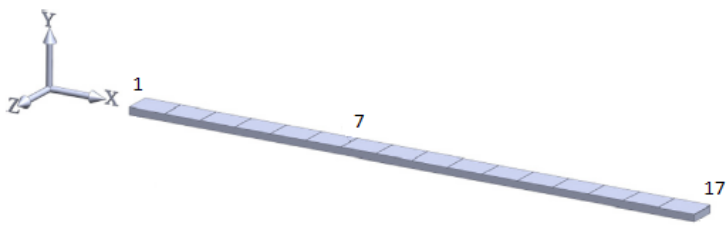

Figure 4.1: Scheme of the beam and its nodes of interest 1, 7 and 17, [22]

This steel beam has a length of $L = 0.8\,m$ and a uniform cross section of $0.02\,m \times 0.005\,m$. The represented nodes of interest 1, 7 and 17 are located along the x axis with coordinates $x_1 = 0m$, $x_7 = 0.3m$ and $x_{17} = 0.8m$ respectively.

The major objectives in this section is to reproduce the TR curves presented in [22], analysing the influence of the mesh on the natural frequencies obtained using the new numerical model and tools created for the present thesis, comparing these with calculated analytical results. Finally, it is also performed a test on the model updating routine based on the TR correlation functions.

4.1.1 Beam Numerical Model

The beam was modeled using ANSYS and is presented in figure 4.2 with 32 FEs. The geometric and elastic properties are presented in table 4.1.

Beam Properties	
Young's modulus - E	$208\,GPa$
Density - ρ	$7840\,kg\,m^{-3}$
Poisson ratio - ν	0.3
Shear coefficient - k	$5/6$
Length - L	$0.8\,m$
Section width - b	$0.005\,m$
Section height - h	$0.02\,m$
Second moment of area - I_z	$2.0833 \times 10^{-10}\,m^4$

Table 4.1: Elastic and geometric beam properties

The shear coefficient value, also known as Timoshenko shear coefficient, normally assumes this value of $k = 5/6$ for beams with constant rectangular cross sections [38]. The beam was modeled in ANSYS using the two-node, 3D Timoshenko beam, where each node has six degrees of freedom $(u_x, u_y, u_z, \theta_x, \theta_x, \theta_z)$, corresponding to *Beam188* as mentioned in chapter 3.

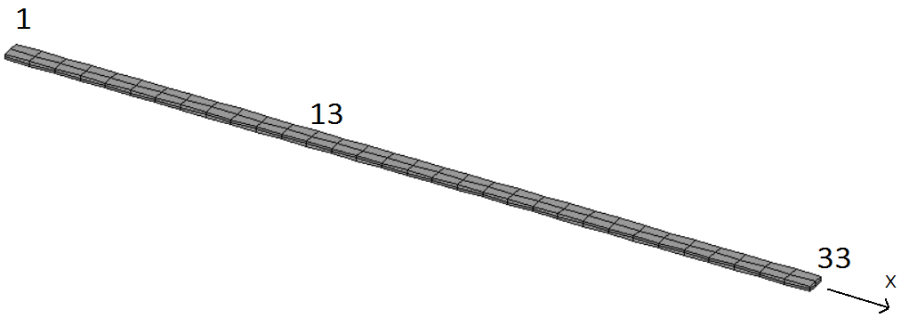

Figure 4.2: Scheme of the beam, nodes of interest 1, 13 and 33

The figure 4.2 illustrates a beam modeled with 32 FEs and also the nodes of interest (1, 13 and 33) , which are represented and positioned in the exact same positions as the nodes considered in the problem of the paper [22].

In order to facilitate the notation, whether we are referring to the model created or the model presented in paper [22], the nodes in the positions $x = 0\,m$, $x = 0.3\,m$ and $x = 0.8\,m$, will always be represented by 1, 13 and 33, respectively. That is, 1 is 1, 13 is 17 and 33 is 17.

In the next section a more detailed analysis on the influence of the mesh refinement will be performed in order to establish the most suitable mesh in terms of number of FEs.

4.1.2 Influence of the Mesh

Before evaluating and testing the updating procedure, one can evaluate the influence of the applied mesh density on the natural frequencies.

Since we are considering a frequency range of $[0Hz, 300Hz]$, the first seven natural frequencies of the modeled beam will be evaluated for increasingly finer meshes.

In agreement with the Timoshenko beam theory, the corresponding first seven natural frequencies will be determined analytically, as presented in section 2.1.2, as a means of comparison with the natural frequencies obtained for each mesh. The MATLAB code used to calculate these natural frequencies is presented in Appendix B.

To perform this analysis, the beam will be successively divided into 8, 16, 32 and 64 FEs. The first seven natural frequencies for each mesh created as well as the analytical ones are presented in the table 4.2.

Analytical (Hz)	**8FE mesh (Hz)**	**16FE mesh (Hz)**	**32FE mesh (Hz)**	**64FE mesh (Hz)**
18,2459	18,2468	18,2459	18,2459	18,2459
72,9689	73,0251	72,9727	72,9693	72,9691
164,1258	164,7440	164,1670	164,1290	164,1270
291,6444	294,9690	291,8710	291,6610	291,6480
455,4241	467,5370	456,2690	455,4840	455,4330
655,3360	689,8830	657,8060	655,5090	655,3580
891,2239	974,3120	897,3090	891,6490	891,2720

Table 4.2: First seven analytical and numerical natural frequencies, increasingly finer meshes (Hz)

As expected, for lower frequency values, the results converge quicker as the mesh is refined, than for higher frequency values.

Providing a more visual perspective on the convergence of these natural frequencies, the graph in figure 4.8 shows the variation of the relative error, of each one of the first seven natural frequencies relative to the corresponding analytical frequencies, with the increasing number of FEs.

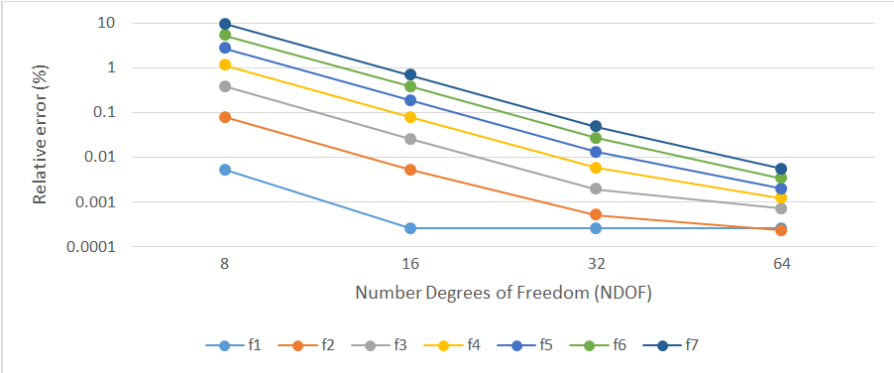

Figure 4.3: Natural frequencies (f_i) relative error vs number of FEs

As can be seen in the graph, there is quite reasonable convergence of all natural frequencies for the beam with 32 FE. The difference for the first 4 natural frequencies, that are within the frequency range of interest, is below the $0.01\,\%$, which is considerably accurate. Taking into consideration the increase in computational cost in case of choosing the 64 FE beam with the minimal increase of accuracy when compared with the 32 FE beam, we come to the conclusion that 32 FEs is a reasonable choice.

Considering frequency range of $[0Hz, 300Hz]$, the following TR curves were obtained both from literature and numerically, as illustrated in figures 4.4 and 4.5, respectively.

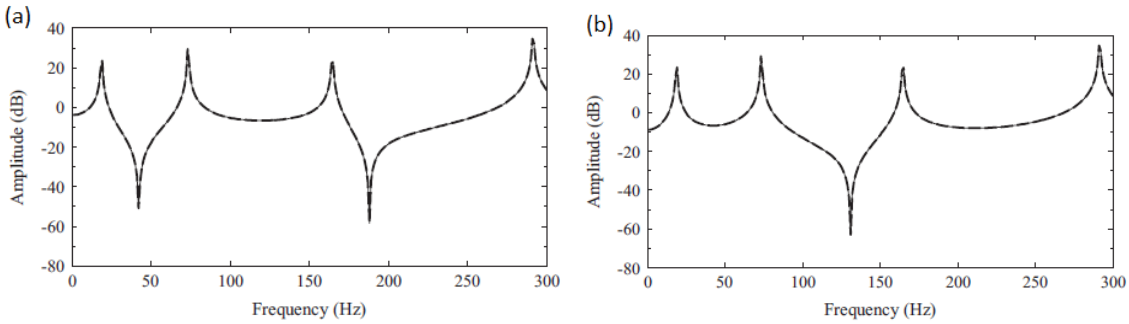

Figure 4.4: TR curves obtained from literature: (a) $T_{1,13}$ and (b) $T_{33,13}$, [22]

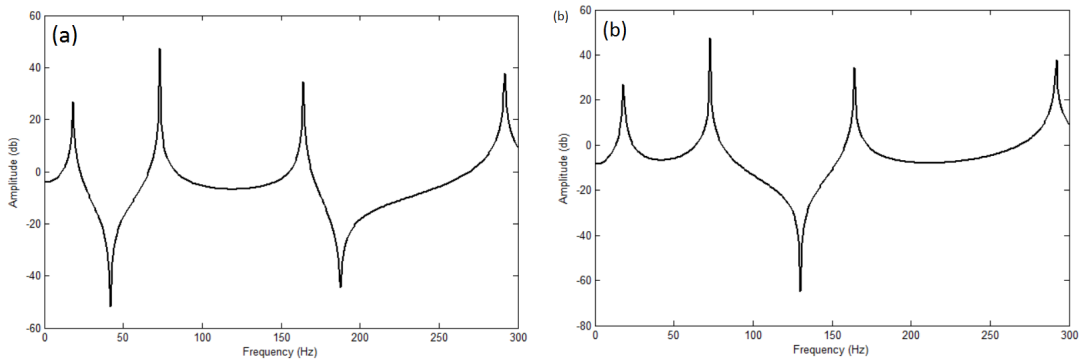

Figure 4.5: TR curves obtained numerically: (a) $T_{1,13}$ and (b) $T_{33,13}$

The dB scale of the TR curves presented above use the unity as reference, $0\ db = 20log_{10}(1/1)$. The

numerical curves were obtained using 300 frequency points.

Comparing the TR curves obtained from literature [22] with the ones obtained numerically, we can verify that there is a practically perfect match of the resonance frequencies in both cases, despite a slight discrepancy in terms of amplitude. A possible reason for this inaccuracy relies on the fact that the numerical models created did not take into consideration any damping, or even just the difference between the number of frequency points considered in both simulations.

4.1.3 Model Updating Procedure Analysis

In this section, the updating procedure based on the TR correlation functions is tested using one and two updating parameters simultaneously.

As explained in the section 3.1.1, the objective function that will be minimized in the updating routine, is based on the two correlation functions presented that measure the level of correlation between the numerical TR data and experimental data.

In this case where we do not have experimental testing data, the two sets of TR data are: the TR reference values, corresponding to the reference beam model as presented in section 4.1.1, and the data corresponding to the reference beam model, except for slight value modifications of the updating parameters of interest. These last TR values will be referred as ”initial” TR. The TR curves used in this updating analysis are $T_{1,13}$ and $T_{33,13}$.

For each updating simulation performed, all the model parameters that are not being updated are set to its corresponding reference values.

The objective function will be minimized, and a good correlation between the two TR curves will be achieved, once the ”initial” updating parameters converge towards the corresponding reference values.

Model Updating Using One Updating Parameter

To start this updating analysis using only one updating parameter, the reference beam length (L) value will be modified to create the ”initial” length value of $L_i = 0.7m$, which will be allowed to vary in between the limit values $[L_l = 0.6m, L_{up} = 0.96m]$.

Similar updating analysis were performed to the beam Young's modulus (E) and section height (h) separately, with initial values of $E_i = 200GPa$ and $h_i = 0.0042m$, and limit values of $[E_l = 166.4GPa, E_{up} = 249.6GPa]$ and $[h_l = 0.004m, h_{up} = 0.006m]$, respectively.

The final updated values for each simulation and the corresponding modulus of the deviations, in respect to the reference value, are represented in the table 4.3.

	Reference	**Initial**	**Updated**	$\Delta_{rel}(\%)$
$L(m)$	0.8	0.7	≈ 0.8	3.8147×10^{-3}
$E(GPa)$	208	200	≈ 207.998	9.390×10^{-4}
$h(m)$	0.005	0.0042	≈ 0.005	2.6855×10^{-3}

Table 4.3: Final updated values L, E and h separately, and reference deviation (%)

For a generic updating parameter P, the reference deviation is given by $\Delta P_{rel}(\%) = |P_{upd} - P_{ref}|/P_{ref} \times 100\ \%$

Model Updating Using Two Updating Parameter

One can now check if the calculated objective function, minimizing the differences between the reference and "initial" TR values, is converging towards a global minimum, taking into account the variation of two updating parameters. These two parameters will be the beam length (L) and section height (h).

As it will be demonstrated next, depending on the updating parameters chosen, the final result of the updating process is somehow dependent on the initial parameter and parameter limit values. In order to achieve meaningful and realistic final results, it is of the utmost importance the correct and suitable application of these limits to the updating parameters values.

To illustrate this situation, two different sets of initial parameter and limit values will be considered in the updating of the beam length (L) and section height (h) as presented in the the table 4.4 presented in table 4.4.

Upd1	**Initial**	**Lower limit**	**Upper limit**
$L(m)$	0.76	0.72	0.88
$h(m)$	0.00530	0.00450	0.00530

Upd2	**Initial**	**Lower limit**	**Upper limit**
$L(m)$	0.77	0.76	0.84
$h(m)$	0.00480	0.00475	0.00525

Table 4.4: Initial and limit values for updating simulations ***Upd1*** and ***Upd2***

The final updated parameters values and the corresponding reference deviations for the two simulations considered, are presented in table 4.5.

	Reference	**Updated *Upd1***	Δ_{rel} ***Upd1*** (%)	**Updated *Upd2***	Δ_{rel} ***Upd2*** (%)
$L(m)$	0.8	≈ 0.81020	1.2744	≈ 0.7950	0.625
$h(m)$	0.005	≈ 0.005128	2.5698	≈ 0.004938	1.2473

Table 4.5: Final updated values L and h simultaneously, and reference deviation (%)

From the previous results, it is clear that the updating procedure works for updating parameters individually, since the final updated parameters values clearly converged to the corresponding reference values as predicted with the reference deviation significantly low.

On the other hand, when updating the beam length and section height simultaneously, the deviations obtained are comparatively higher when comparing with individual parameter updating.

It is presented in figure 4.6 the graphs corresponding to the TR and final updating correlation curves for the simulation ***Upd1***. As we can confirm, even though the TR updated curve (dashed line) and the

reference (full line) are perfectly coincident, there are definitely some amplitude discrepancies between the two close to the natural frequency $73Hz$.

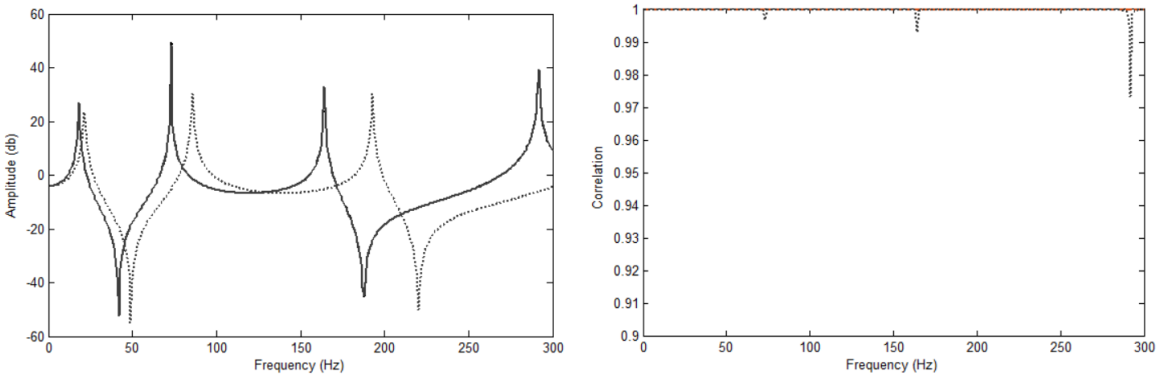

Figure 4.6: Left: Reference (full line), "Initial" (dotted) and Updated (dashed) $T_{1,13}$ TR curves; Right: Final Correlation curve simulation ***Upd1***: $CSAC(\omega)$ (orange dashed line) and $CSF(\omega)$ (black dotted line), TR Updating of L and h

Therefore, we can conclude that even thought the updating procedure may produce results that satisfy our requirements in terms of FRF or TR curve fitting, the limits applied to the chosen updating parameter, is very important when it comes to achieve a suitable and physically meaningful final updated model.

4.2 Experimental Beam Model Updating

In this section, the model updating procedure will be performed using FRF and TR results extracted experimentally from a beam structure (see figure 4.7).

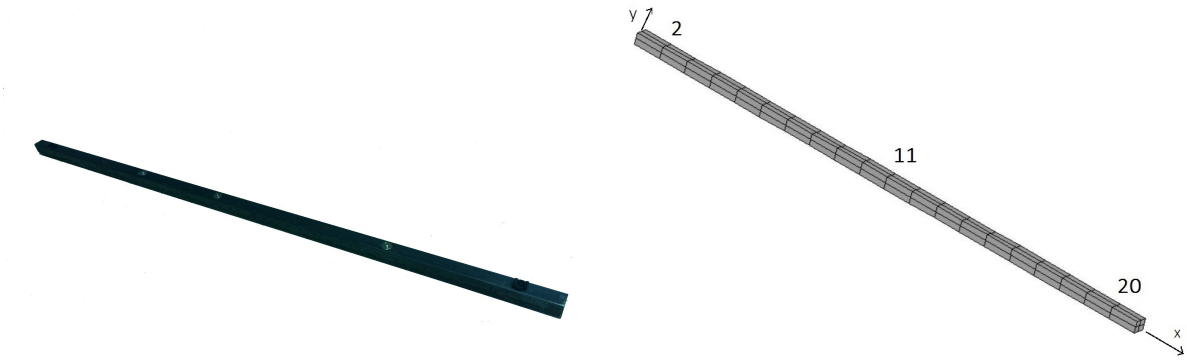

Figure 4.7: Experimental (left) and finite Element beam (right) models

Using the FRF model updating procedure, the influence of the number of modes, considered when calculating the FRF curves, in the final updated results will be inspected, using only one parameter. Afterwards, these results will be compared with results obtained from the TR model updating procedure using the same updating parameters.

In the next two subsections, the numerical model of the beam will be explained in more detail and a simple analysis will be performed on the influence of the mesh on the natural frequencies within the range of interest, assuming simply supported BC, in order to establish the best mesh refinement for the updating.

4.2.1 Experimental Beam Numerical Model

The geometric and elastic properties of the beam are presented in table 4.6. The FE model was created in ANSYS using the dimensions measured in the laboratory, and the material assumed was a structural steel.

Beam Properties	
Young's modulus - E	$208\,GPa$
Density - ρ	$7840\,kg\,m^{-3}$
Poisson ratio - ν	0.3
Shear coefficient - k	$5/6$
Length - L	$0.975\,m$
Section width - b	$0.02\,m$
Section height - h	$0.02\,m$
Second moment of area - I_z	$1.333 \times 10^{-8}\,m^4$

Table 4.6: Elastic and geometric beam properties

The beam element used in ANSYS was a two-node, 3D Timoshenko element, where each node has six DOFs $(u_x, u_y, u_z, \theta_x, \theta_y, \theta_z)$, corresponding to *Beam188* as mentioned in chapter 3.

The represented nodes of interest 2, 11 and 20 in figure 4.7 are located along the x axis with coordinates $x_2 = 0.04875\,m$, $x_{11} = 0.4875\,m$ and $x_{20} = 0.92625\,m$, respectively.

4.2.2 Influence of the Mesh

The influence of the applied mesh density to the FE model on the first natural frequencies of the structure will be evaluated, in order to establish the most suitable mesh in terms of number of number of finitte elements.

According to the Timoshenko beam theory for a simply supported beam, the first four natural frequencies of the model were determined analytically, as presented in section 2.1.2, as a means of comparison with the natural frequencies obtained for each mesh.

The first four natural frequencies obtained numerically with ANSYS, were obtained successively dividing the model into 10, 20 and 40 FEs. The analytical and numerical frequencies for each model are presented in the table below:

Analytical (Hz)	**10FE mesh** (Hz)	**20FE mesh** (Hz)	**40FE mesh** (Hz)
49,3622	49,3635	49,3625	49,3625
197,0290	197,096	197,037	197,034
441,7576	442,469	441,824	441,782
781,5298	785,319	781,843	781,614

Table 4.7: First four analytical and numerical natural frequencies, increasingly finer mesh (Hz)

As expected, for lower frequency values, the frequency values converge much quicker as the number of FEs is increased, than for higher frequencies.

The graph below shows the variation of the relative difference, of each one of the first four natural frequencies relative to the corresponding analytical frequencies, with the increasing number of finite elements.

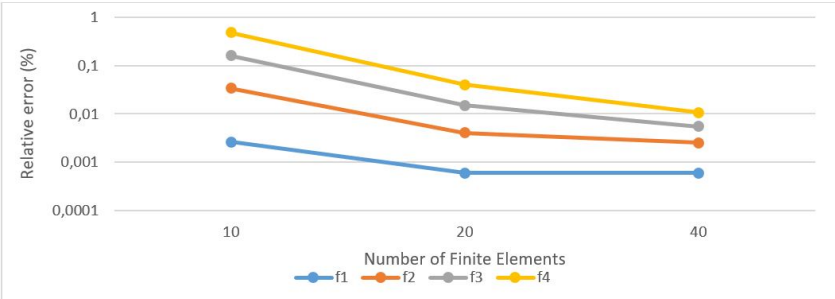

Figure 4.8: Natural frequencies (f_i) relative difference vs number of FEs

Taking into consideration that the frequency range of interest in the following model updating simulations is quite low ($0Hz$ to about $180Hz$), the chosen mesh will be the 20 FE mesh. The first two natural frequencies, that are the closest too the frequency range of interest, present an error below $0.01\,\%$, which is quite accurate.

The alternative of choosing the 40 FE mesh instead of the 20 FE mesh, would imply an increase in the computational cost in exchange for a small increase in the results accuracy.

4.2.3 Frequency Response Function Model Updating

In this section, the FRF model updating procedure will be applied to the beam structure introduced in section 4.2.1.

The updating methodology, as explained in section 3.1.1, is based on the FRF correlation functions.

The 20 FEs model created with the properties defined in section 4.2.1 will be referred as the reference model. Depending on the updating parameter considered in the simulation, a small modification will be applied to this variable of interest, originating what will be referred to as the initial model.

This small value change in the updating parameter of interest allows us to have a better numerical and even visual perception of what happens with this value during the updating process and towards

which value does it converge.

Finally, the resulting model from the updating process, will be referred as the final model or updated model and the experimental results referred simply as experimental model.

The frequency range considered in all FRF model updating simulations is $[0\,Hz, 200\,Hz]$ and for both experimental and numerical data, the frequency interval increment is $0.5\,Hz$, meaning in this case that 400 frequency points will be used to plot the FRF curves.

While extracting the FRF amplitude values for a specified frequency range, five different measurements are performed to obtain each curve. Therefore, the coherence between these five measurements gives us a clear indication on the quality of the results extracted, so that if this average is satisfactorily close to one (perfect coherence), it means all measurements were consistent with each other in the frequency range considered.

The FRF used in the updating process will be $H_{2,2}$ and $H_{20,2}$. These FRF curves were selected instead of the others because of the acceptable quality of extraction of these results in comparison with others.

To illustrate this situation, two experimental measurement coherence curves are presented in figure 4.9.

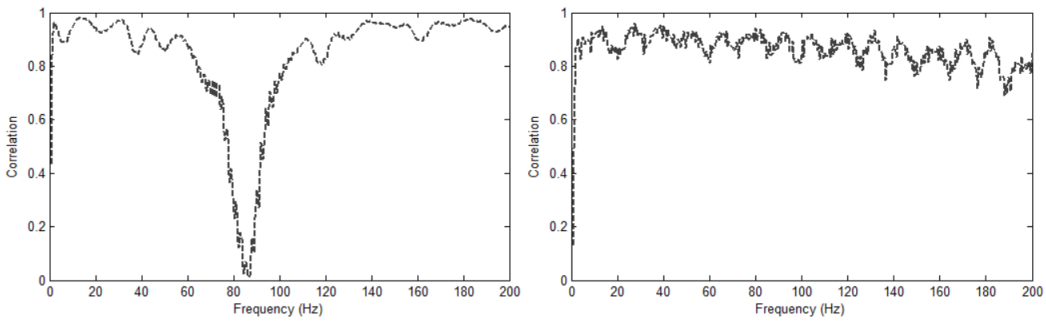

Figure 4.9: $H_{2,2}$ and $H_{2,20}$ experimental FRF measurements coherence functions

The coherence of the measurements for the FRF $H_{2,2}$, which will be used in the updating simulations, presents satisfactory values up to $200\,Hz$.

The coherence of the measurements for the FRF $H_{2,20}$, which will not be used in the updating simulations, presents some noise throughout the frequency range considered and the correlation get relatively worst with the increase of the frequency.

Model Updating Using One Updating Parameter

We will now investigate the influence of the number of modes considered when calculating the FRF amplitude values on the final updated results, using one and two updating parameters simultaneously in a simulation, see section 2.3.3.

The first updating parameter considered is the beam length (L). The initial model corresponds to a initial length value (L_i) as presented table 4.8. The limits, for the length value during the updating procedure, are also presented below:

	Initial	Lower limit	Upper limit
L (m)	0.90	0.8775	1.0725

Table 4.8: Initial and limit values for L, FRF updating

Three simulations will be performed using 6 (**m6**), 12 (**m12**) and 24 (**m24**) modes to calculate the the frequency response functions.

The final updated length values (L_{upd}) for each of the updating simulations as well as the deviation in respect to the reference length value ($\Delta L_{rel}(\%) = |(L_{ref} - L_{upd})/L_{ref}| \times 100\%$) are presented in the table 4.24.

	Reference	Upd. m6	Δ_{rel} (%)	Upd. m12	Δ_{rel} (%)	Upd. m24	Δ_{rel} (%)
L (m)	0.975	0.97257	0.2491	0.97250	0.2582	0.97250	0.2582
time (s)		840.15		834.48		888.73	

Table 4.9: Final updated value of L, and reference deviation (%), FRF updating for simulations **m6**, **m12** and **m24**

There is not much difference between the final updated length values in the three cases considered, resulting in almost identical final updated FRF curves. Despite this fact, one can verify that there is a slight change in the reference deviation from **m6** to **m12** stabilizing in **m24**, probably meaning that the final updated value is converging to a global minimum with the increase of precision.

The initial, experimental and updated final FRF curves for both $H_{2,2}$ and $H_{20,2}$ amplitude values, as well as the initial and final correlation functions (both $CSAC(\omega)$ and $CSF(\omega)$ correlation function) are presented in figures 4.10 and 4.11 for the twelve modes simulation (**m12**).

These initial and final correlation curves represent the correlation between the experimental and initial model and the experimental and final updated model, respectively.

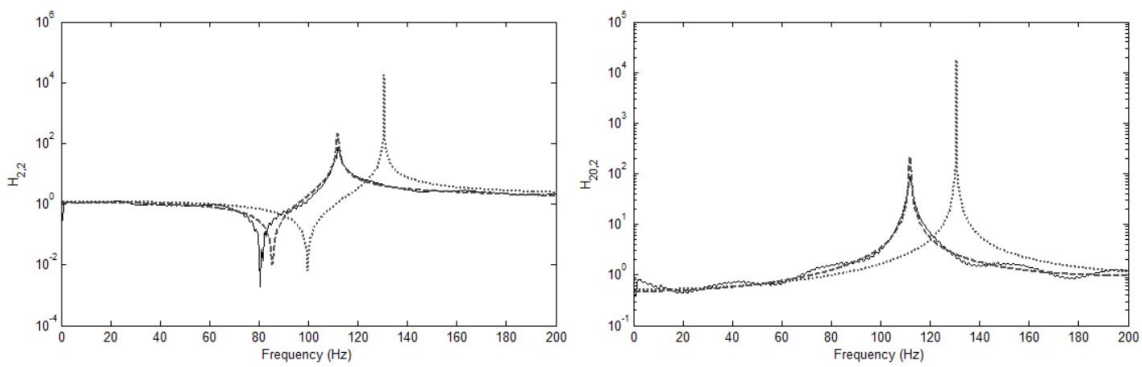

Figure 4.10: Initial (dotted line), experimental (full line) and updated (dashed line) $H_{2,2}$ (left) and $H_{20,2}$ (right), updating L, **m12**, FRF updating

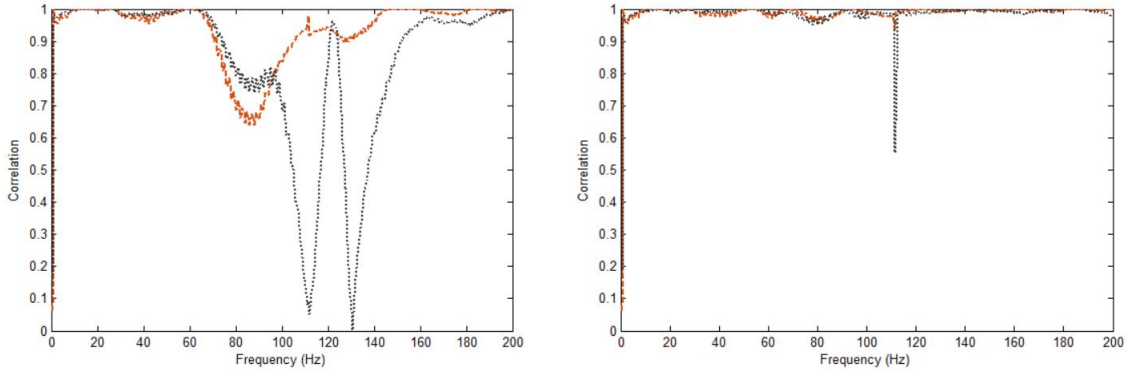

Figure 4.11: Initial (left) and final (right) correlation functions $CSAC(\omega)$ (orange dashed line) and $CSF(\omega)$ (black dotted line), updating L, **m12**, FRF updating

Except for some small oscillations of the experimental FRF values, it can be verified that an almost perfect fit between the final and experimental FRF curves is achieved.

This statement is corroborated with the final correlation functions values (see figure 4.11, right), that evaluate the amplitude and overall shape correlation between the experimental and final updated curve of both FRF curves. The valley of the CSF function curve, corresponding to the resonance frequency (approximately $111\,Hz$), occurs because of the discrepancy between experimental an final FRFs curves. This discrepancy can be explained by the fact that, despite all real vibrating structures having, even if very little, damping mechanisms, it was assumed no damping for the numerical models.

Similarly, using 6, 12 and 24 modes to obtain the FRF values, three updating simulations (**m6**, **m12** and **m24**, respectively) were performed, but this time using the Young's modulus (E) as the updating parameter.

The initial and limit values for E are presented in table 4.10. The final updated results and the reference deviation, for each one of the three simulations, are also given below in table 4.11.

	Initial	**Lower limit**	**Upper limit**
E (GPa)	190	187.2	228.8

Table 4.10: Initial and limit values of L, FRF updating

	Reference	**Upd. m6**	Δ_{rel} (%)	**Upd. m12**	Δ_{rel} (%)	**Upd. m24**	Δ_{rel} (%)
E (GPa)	208	210.039	0.9802	210.147	1.0321	210.090	1.0044
time (s)		286.77		277.36		342.85	

Table 4.11: Final updated value of E and reference deviation (%), FRF updating for simulations **m6**, **m12** and **m24**

Once again, one can verify that the increase in the number of modes considered, doesn't change significantly the final updated value of the updating parameter of interest E.

The initial, experimental and updated final FRF curves for both $H_{2,2}$ and $H_{20,2}$ amplitude values, as

well as the initial and final correlation functions are presented in figures 4.12 and 4.13 below for the twelve modes updating simulation (**m12**).

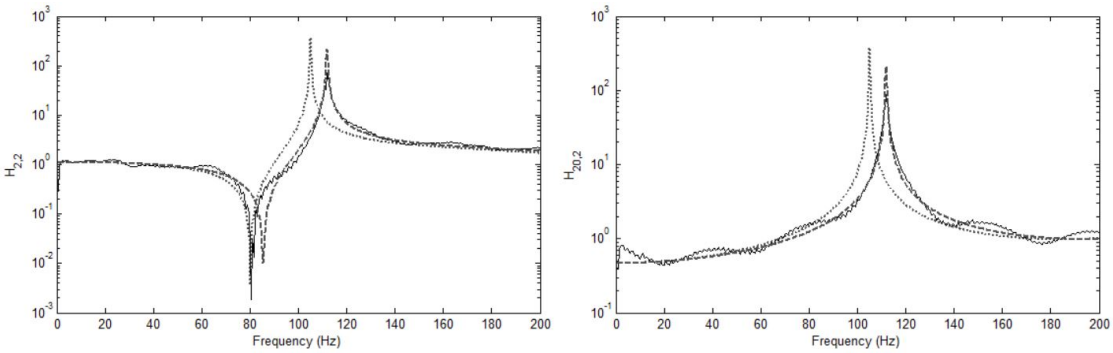

Figure 4.12: Initial (dotted line), experimental (full line) and updated (dashed line) $H_{2,2}$ (left) and $H_{20,2}$ (right), updating E, **m12**, FRF updating

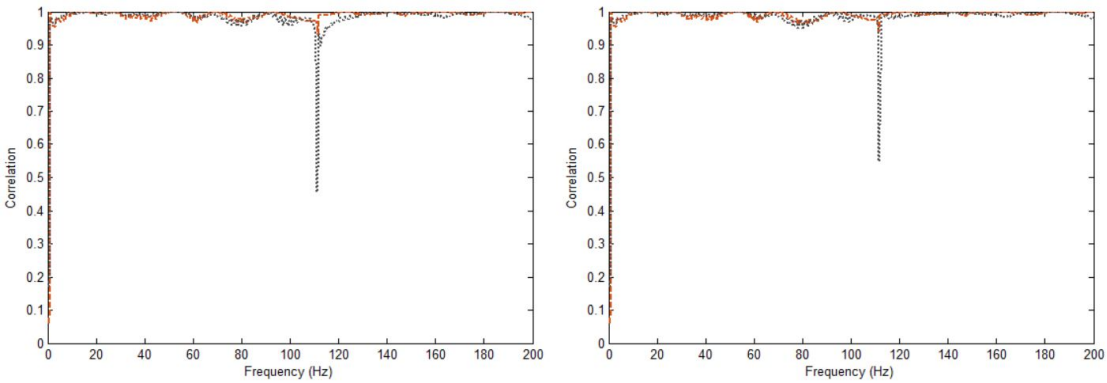

Figure 4.13: Initial (left) and final (right) correlation functions $CSAC(\omega)$ (orange dashed line) and $CSF(\omega)$ (black dotted line), updating E, **m12**, FRF updating

The difference between the initial and final correlations is not visually significant. Nevertheless, similar to what happened when updating the beam length, there is an almost perfect overlap of the experimental and final FRF curves, except for some small oscillations and an amplitude discrepancy close too the resonance frequency (approximately $111\,Hz$).

The simulations times for the beam length updating simulations are considerably greater that for the Young's modulus updating.

Although the simulation times are relatively short,one can notice as expected that there is an increase in the computational time when comparing the simulation using 6 modes and the one using 24 modes.

Performing a model updating analysis to a larger FE model, with a higher number of DOFs, implies an increase of the computational cost when compared with this simple beam structure simulations. Depending on the simulation objectives and final goals, a trade-off between computational cost and results accuracy is very important, especially for large structures.

Model Updating Using Two Updating Parameter

The model updating procedure will now be tested using two updating parameters, considering twelve modes when calculating the FRF values (**m12**). The updating parameters used in this simulation will once again be the beam length (L) and Young's modulus (E).

The initial parameter and limit values for this simulation are presented in table 4.12. The final updated results of both parameters as well as the relative difference, in respect to the reference parameter values, are also given below in table 4.13.

	Initial	**Lower limit**	**Upper limit**
L (m)	0.90	0.8775	1.0725
E (GPa)	190	187.2	228.8

Table 4.12: Initial and limit values of L and E, FRF updating

	Reference	**Upd. m12**	Δ_{rel} **m12** (%)
L (m)	0.975	0.9609	1.4423
E (GPa)	208	198.169	4.7266
time (s)		768.93	

Table 4.13: Final updated values of L and E simultaneously, and reference deviation (%), FRF updating for **m12**

The initial, experimental and updated final FRF curves for both $H_{2,2}$ and $H_{20,2}$ amplitude values, as well as the initial and final correlation functions are presented in figures 4.14 and 4.15.

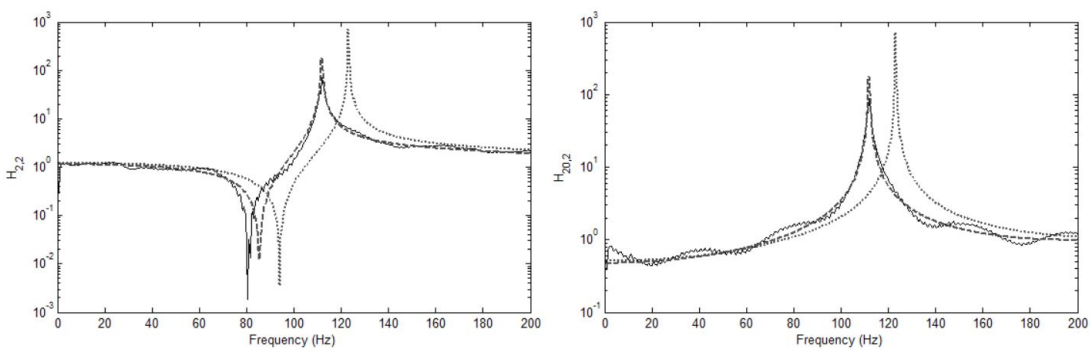

Figure 4.14: Initial (dotted line), experimental (full line) and updated (dashed line) $H_{2,2}$ (left) and $H_{20,2}$ (right), Updating L and E, FRF updating

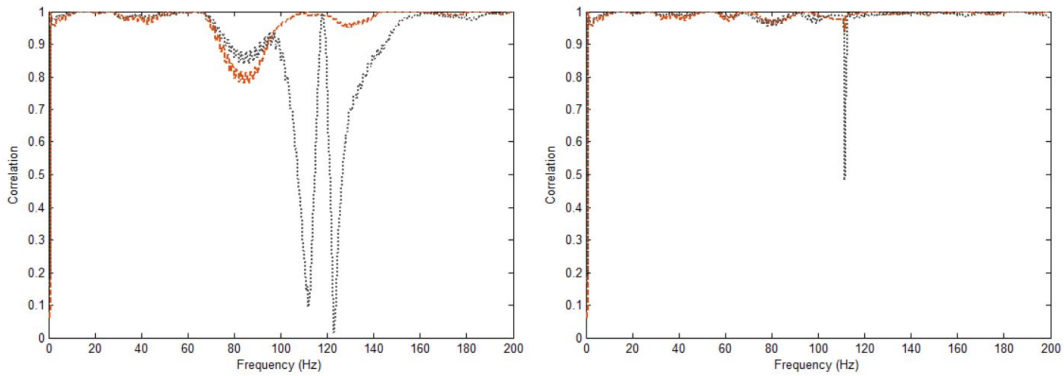

Figure 4.15: Initial (left) and final (right) correlation functions $CSAC(\omega)$ (orange dashed line) and $CSF(\omega)$ (black dotted line), Updating L and E, FRF updating

The final updated parameter values for this simulation using two updating parameters are slightly different from the ones obtained updating each one of these parameters individually. However, more specifically for the beam length (L), the final updated values in both cases diverge a maximum of approximately $1.5\,\%$ from the measured beam length, $L_{ref} = 0.975\,m$.

Overall, we can conclude that this updating procedure, based on the FRF correlation functions, works both for updating parameters individually and simultaneously rather effectively. Given appropriate limit values for the updating parameters of interest, the updating procedure developed will ultimately gives us a final model that best fits the experimental model, in terms of the frequency response functions curves considered.

4.2.4 Transmissibility Model Updating

In this section the transmissibility model updating procedure will be applied to the beam structure using once again one and two updating parameters. The updating parameters considered will be the same beam length (L) and Young's modulus (E).

The transmissibility curves used throughout this section are $T_{2,11}(\omega)$ and $T_{20,11}(\omega)$. The meaning of these TRs can be explained as the amplitude of the force transmitted to nodes 2 and 20 (y direction) when a force with amplitude of $1\,N$ is applied to node 11 (y direction), respectively, for each value of the frequency range considered.

The frequency range considered in the following TR updating simulations is $[0\,Hz,\,100\,Hz]$ and for both experimental and numerical data, the frequency interval increment is $0.5\,Hz$, meaning in this case 200 frequency points will be used to plot the TR function curves.

As discussed in section 4.2.3, some experimental FRF curves obtained experimentally, show a considerable low level of coherence between the five measurements performed to obtain each of the FRF curves. See the example of the correlation curve for the extraction of the $H_{2,20}$ FRF curve in figure 4.9.

The frequency range limit considered in the FRF updating simulations was $200\,Hz$. Experimentally, for frequency values approximately beyond the stated limit of $100\,Hz$, these FRF values start oscillating, even if very little. Since the TR values are calculated as the ratio of two FRF values, these oscillations and noise appear catalysed in the calculated TR curves as these irregularities start to appear specially for higher frequency values.

Despite the quality of the extracted experimental results, in the following sections, it will be demonstrated that the updating procedure based on the correlation of the TR curves, works quite properly using one and two updating parameters simultaneously.

Model Updating Using One Updating Parameter

The updating parameters, L and E, will be used to updated the same structure, only this time the updating procedure is focused in maximizing the correlation between the chosen TR curves obtained experimentally and the corresponding curves obtained numerically.

Bearing in mind that these parameters will be used to update the numerical model, in two separate simulations, the table 4.14 presents the initial simulation values and the limit values for each of the updating simulations. The final updated results of both simulations as well as the deviation in respect to the reference parameter value, are presented in table 4.15. All the following updating simulations will be using 12 modes (**m12**) to calculate the FRF values and consequently the TR function values, see section 2.3.3.

	Initial	**Lower limit**	**Upper limit**
L (m)	0.90	0.8775	1.0725
E (GPa)	190	187.2	228.8

Table 4.14: Initial and limit values of L and E, TR updating

	Reference	**Upd. m12**	Δ_{rel} **m12** (%)
L (m)	0.975	0.9600	1.540
E (GPa)	208	221.450	6.4665

Table 4.15: Final updated values of L and E separately, and reference deviation (%), TR updating for **m12**

The initial, experimental and updated final TR curves for both $T_{2,11}$ and $T_{20,11}$ amplitude values, as well as the initial and final correlation functions for the updating of the beam length (L), are presented in figures 4.16 and 4.17.

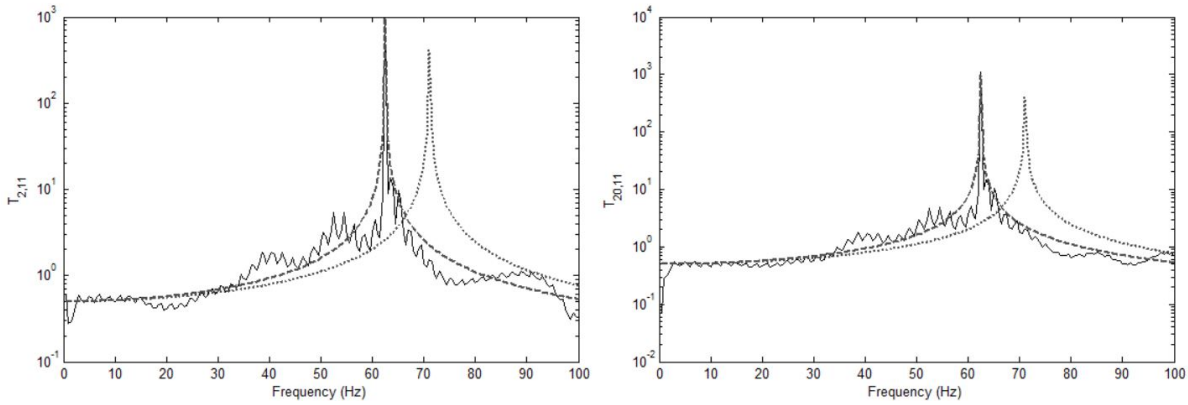

Figure 4.16: Initial (dotted line), experimental (full line) and updated (dashed line) $T_{2,11}$ (left) and $T_{20,11}$ (right), Updating L, TR updating

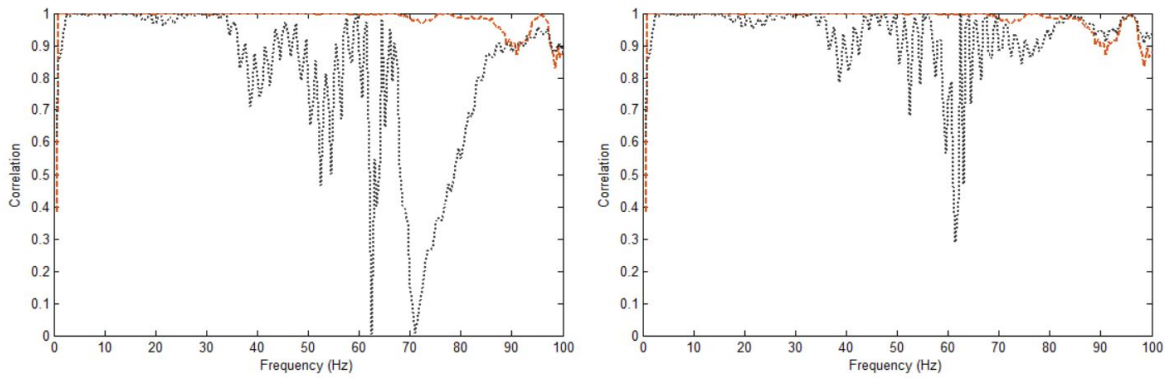

Figure 4.17: Initial (left) and final (right) correlation functions $CSAC(\omega)$ (orange dashed line) and $CSF(\omega)$ (black dotted line), Updating L, TR updating

The corresponding curves for the Young's modulus (E) updating simulation are presented in figures 4.18 and 4.19.

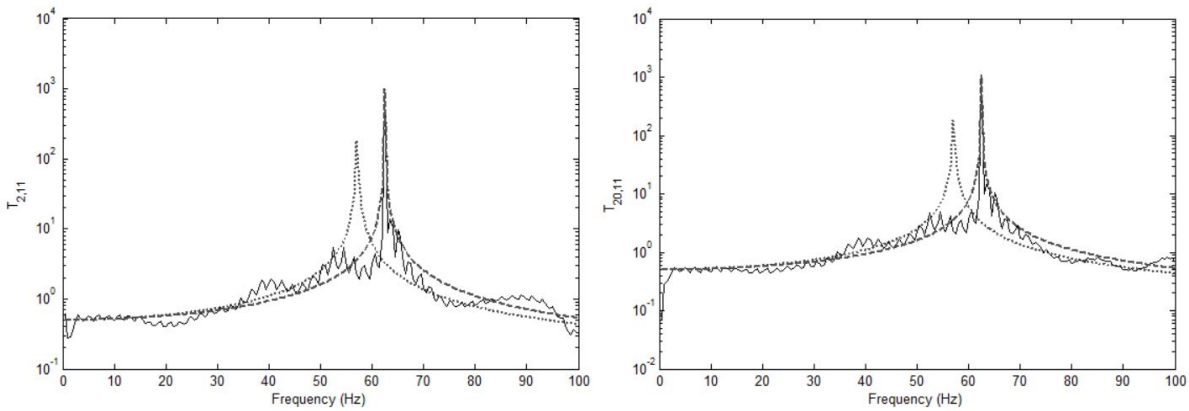

Figure 4.18: Initial (dotted line), experimental (full line) and updated (dashed line) $T_{2,11}$ (left) and $T_{20,11}$ (right), Updating E, TR updating

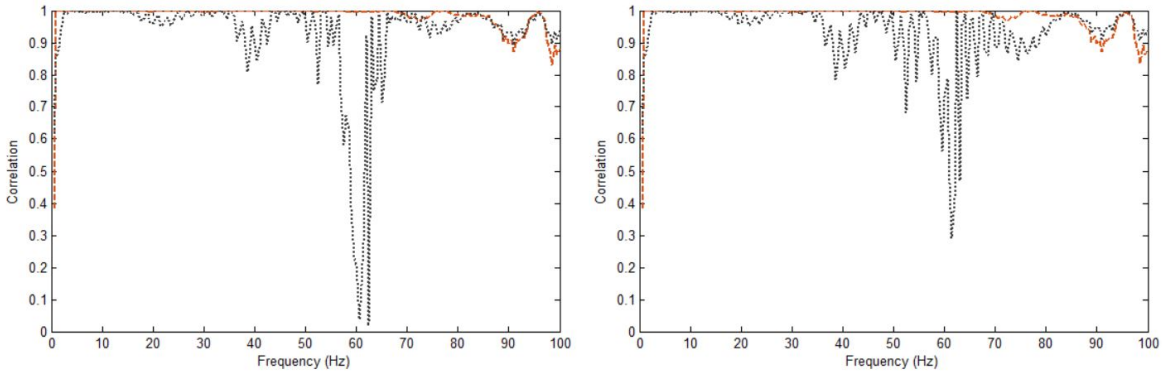

Figure 4.19: Initial (left) and final (right) correlation functions $CSAC(\omega)$ (orange dashed line) and $CSF(\omega)$ (black dotted line), Updating E, TR updating

The results of both updating simulations show that, despite imperfections in the experimental results (noise and oscillations), there is a near overlap between the experimental and updated curves in both TR curves ($T_{2,11}$ (left) and $T_{20,11}$ (right)), in terms of the overall curve shape.

The final updated value obtained for the beam length of $L_{upd} = 0.96\,m$ is quite acceptable considering that the measured length is $L_{ref} = 0.975\,m$. On the other hand, the final updated value for the Young's modulus $E_{upd} = 221.45\,GPa$ is relatively higher according to what is expected.

From the initial and final correlation functions, one can also verify that there was a clear increase in the global correlation between the numerical and experimental curves.

Model Updating Using Two Updating Parameter

The model updating procedure based on TR functions, will now be tested using two updating parameters. The parameters used in this simulation will be once again the beam length (L) and Young's modulus (E).

The initial simulation values and the limit values for both parameters are presented in the table 4.14. The final updated results as well as the deviation in respect to the reference parameters values, are presented in table 4.16.

	Reference	**Upd. m12**	Δ_{rel} **m12** (%)
L (m)	0.975	0.9710	0.4102
E (GPa)	208	217.811	4.7170

Table 4.16: Final updated values of L and E simultaneously, and reference deviation (%), TR updating for **m12**

The initial, experimental and updated final TR curves for both $T_{2,11}$ and $T_{20,11}$ amplitude values, as well as the initial and final correlation functions for the updating of the beam length (L)and Young's modulus (E), are presented in figures 4.20 and 4.21.

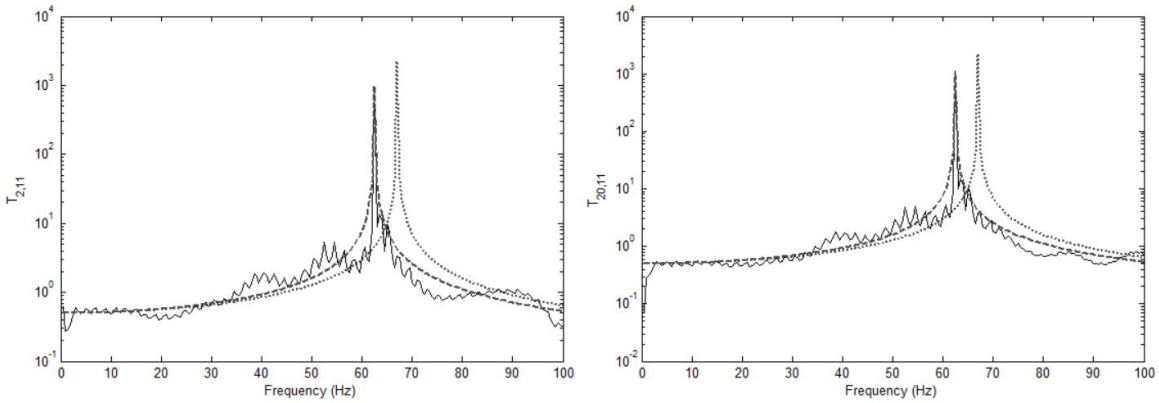

Figure 4.20: Initial (dotted line), experimental (full line) and updated (dashed line) $T_{2,11}$ (left) and $T_{20,11}$ (right), Updating L and E, TR updating

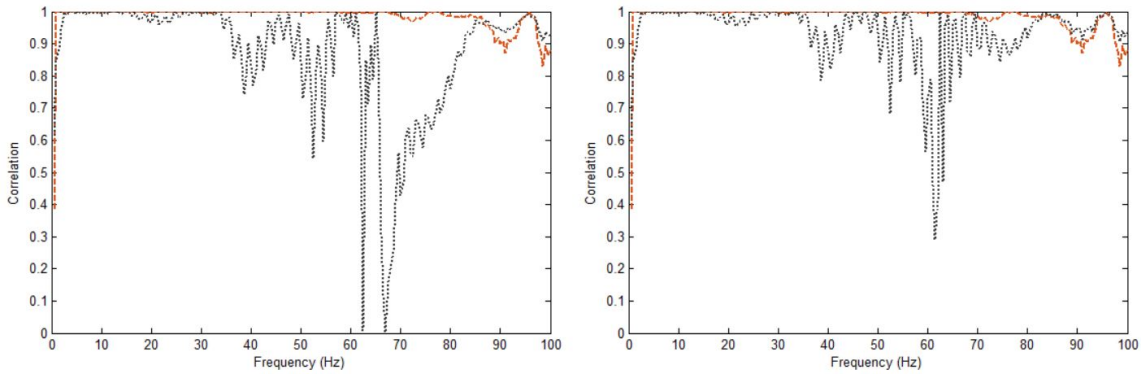

Figure 4.21: Initial (left) and final (right) correlation functions $CSAC(\omega)$ (orange dashed line) and $CSF(\omega)$ (black dotted line), Updating L and E, TR updating

The final updated parameter values obtained in simulation using the two updating parameters are slightly different from the ones obtained when updating each one of these parameters individually. However, analogously to what happened in the FRF updating simulations, the final updated values of the beam length, whether updated separately or together with the Young's modulus, diverge a maximum of approximately $1.5\,\%$ from the measured beam length value of $L_{ref} = 0.975\,m$.

Globally, one can conclude that this updating procedure, based no the TR correlation functions, works appropriately for updating both one parameter individually and two parameters simultaneously, giving us acceptable updated results within the specified limit values.

The final updated parameter values obtained using the FRF-based and TR-based methodologies are slightly different, whether using one and two updating parameters simultaneously.

For the individual updating of L and E, one can verify that the FRF-based updating produced results closer to the measured length and expected Young modulus values, when compared with the TR-based updating. On the other hand, updating the two parameters simultaneously, the TR-based updating methodology resulted in a beam length value $L_{upd} = 0.9710\,m$ closer to the measured length of reference $L_{ref} = 0.975\,m$.

4.3 Simplified Aircraft Model

A benchmark study is presented in [39], which objective is to compare the results obtained using different computational model updating procedures for a common structure. The participants in this study would have to comply with a series of requirements including the correct prediction of the experimental and/or frequency response functions of the model generated by each group, within the frequency range of interest.

The objective of this study was to validate the model using the test data made available to the participants. These data included 24 FRFs from the university of Manchester (**U_MAN**) and modal data between $6.376\,Hz$ (mode 1) and $151.317\,Hz$ provided by **DLR**, Göttinggen, Germany. The Imperial College of Science (**IC**) re-tested the structure in order to obtain the same 24 FRF as **U_MAN**.

The common structure used in this study is a simplified aircraft structure as presented in figure 4.22.

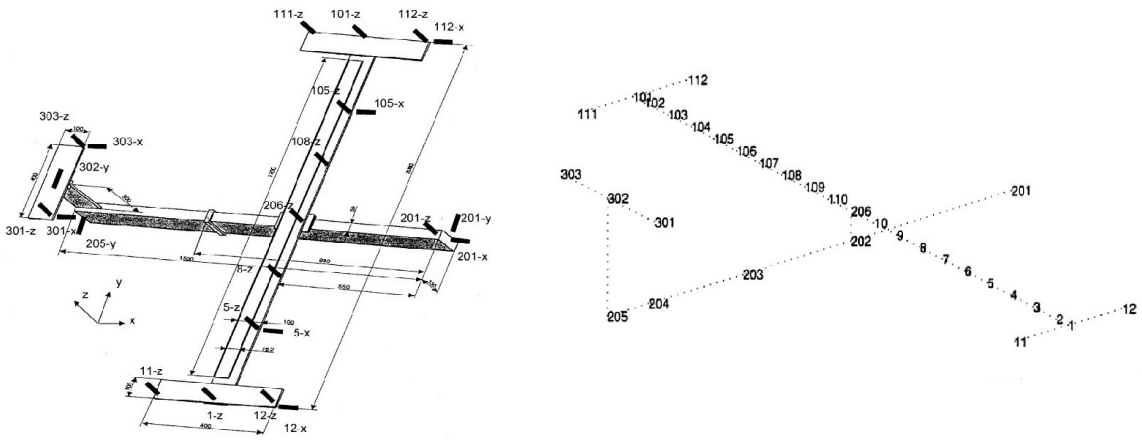

Figure 4.22: Aircraft structure used in the validation benchmark study - GATEUR SM-AG19 (left, [39]); Initial FE model proposed in [40] (right)

The only test data available to us was the modal data provided by **DLR** and three example of FRFs curves from **IC** and **U_MAN**. These results will simply serve as a means of visual comparison with the results obtained from the numerical FE model created.

The major objective is to conclude about the accuracy of the numerical model generated and also the viability of representing a structure like this, using such a simplified FE modelling approach.

4.3.1 Aircraft Numerical Model

A reference FE model is given in [40] in order to give a common basis for the analytical studies.

Although this model uses simple beam elements, as it will be verified, the predictions are quite good.

This model will be our basic reference model used in this section. The material assumed was aluminium as suggested. The properties of the FE model generated are presented in table 4.17.

Material Properties	
Young's modulus - E	$72\,GPa$
Density - ρ	$2700\,kgm^{-3}$
Poisson ratio - ν	0.3
Shear coefficient - k	$5/6$

Table 4.17: Aircraft material properties, aluminium

The FE model was modeled in ANSYS with 32 FEs and 33 nodes (see figure 4.23), using two-node, 3D Timoshenko beam elements. Each node has six degrees of freedom $(u_x, x_y, u_z, \theta_x, \theta_y, \theta_z)$.

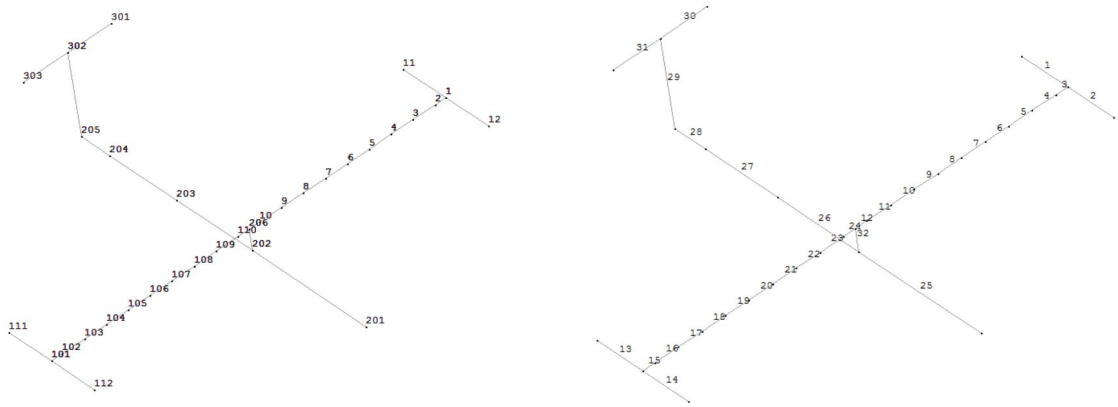

Figure 4.23: ANSYS FE model and nodes (left) and elements (right) numbering schemes

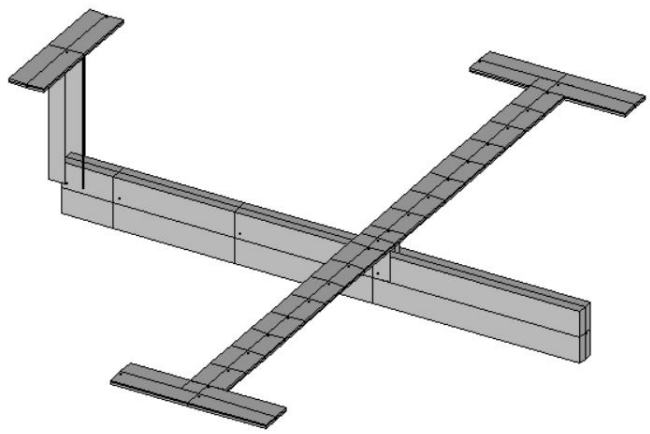

Figure 4.24: ANSYS FE model scheme

In order to give the final dimension of the FE model, the structures was divided into six major regions. Figure 4.23 presents the numbering schemes for the nodes and elements of the aircraft structure. Region 1 corresponds to the aircraft wing (elements $3-12$ and $15-24$), region 2 the wing tips (elements 1, 2, 13 and 14) and region 3 the fuselage (elements $25-28$). Vertical and horizontal tails correspond

to regions 4 and 5 (elements 29 and $30-31$), respectively. Region 6 is the wing off-set in the z direction, which can be observed in figure 4.23 (element 32). Table 4.21 below show the lengths and the rectangular cross sectional dimensions for each of these regions:

Region	b (m)	h (m)	L (m)
1 (wing)	0.1	0.01	1.8
2 (wing tips)	0.1	0.01	0.45
3 (fuselage)	0.15	0.05	1.5
4 (vertical tail)	0.1	0.01	0.381
5 (horizontal tail)	0.1	0.01	0.4
6 (wing off-set)	0.1	0.05	0.096

Table 4.18: Dimensions of lengths (L), section width (b) and height (h) of the six aircraft sections

In the next section, the modal and FRFs data obtained using the generated FE model is compared with the corresponding results presented in literature.

4.3.2 Finite Element Model Analysis

The first six numerical eigenfrequencies obtained using ANSYS are presented in the table 4.19 together with the corresponding eigenfrequency obtained from literature [39]. The deviations in percentage of numerical frequencies obtained in respect to the literature frequency values are also presented.

Mode	1	2	3	4	5	6
Literature (Hz)	6.4	16.1	33.1	33.5	35.7	48.4
Numerical (Hz)	6.36334	15.9291	33.8384	33.9246	34.6512	49.589
Difference (%)	0.572813	1.061491	-2.23082	-1.26746	2.937815	-2.45661

Table 4.19: Eigenfrequency values obtained from literature numerically and the corresponding reference deviation (%)

The first six mode shapes obtained numerically, along with the corresponding values of frequency, are presented in figure 4.25. The corresponding mode shapes available in literature [39] are presented below in figure 4.26.

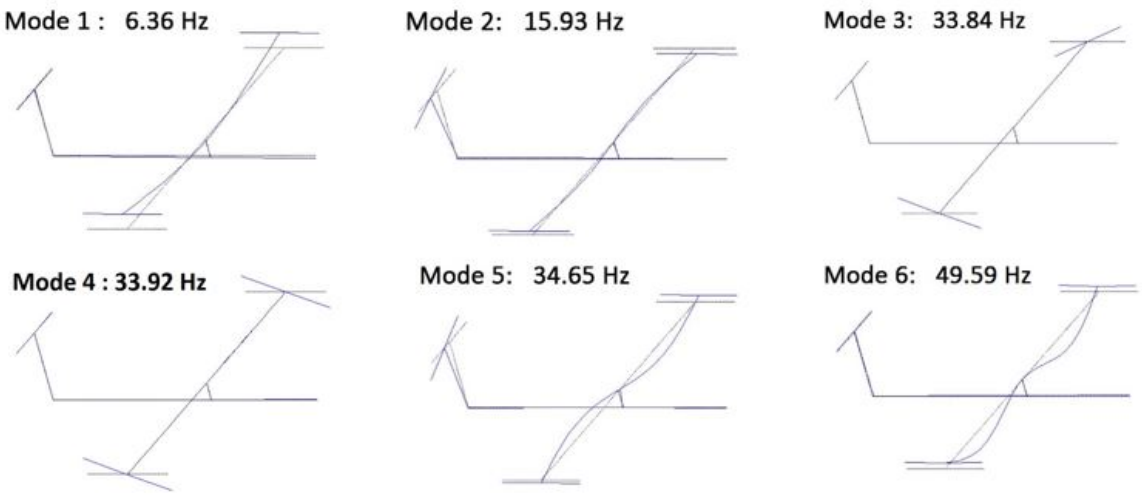

Figure 4.25: First six mode shapes and corresponding frequency measured by **DLR**, [39]

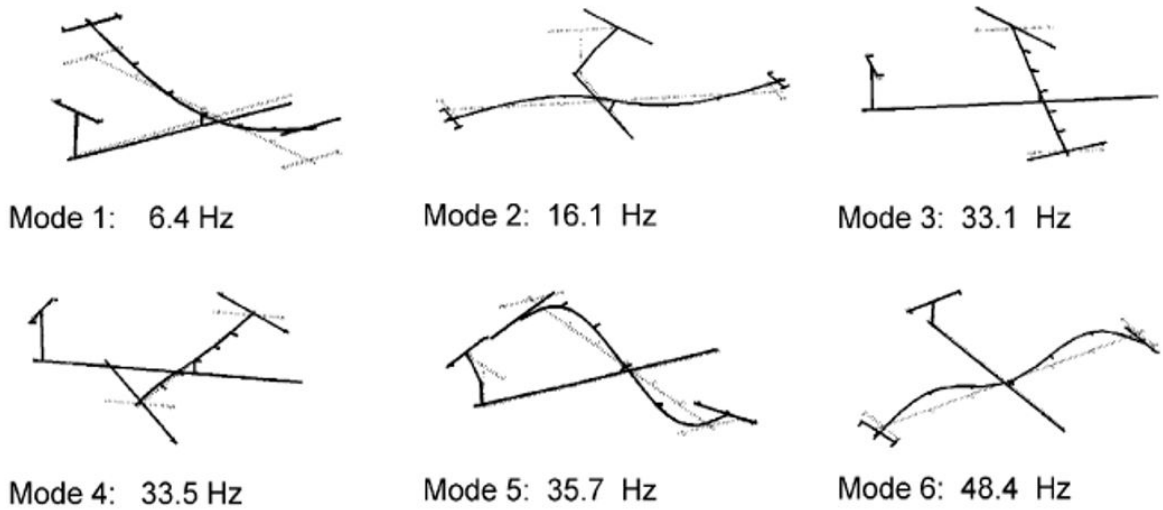

Figure 4.26: First six mode shapes and corresponding frequencies obtained using ANSYS

As stated at the beginning of this section, three examples of FRF curves were available to us, from the **U_MAN** and **IC** testing.

Considering the referential presented in figure 4.22 and the node numbering notation presented in figure 4.23, the FRFs curves presented below correspond to accelerance measurements at the DOF $12z$, $112x$ and $205y$ due to excitation at the right wing tip, $12z$ ($H_{12z,12z}$, $H_{112x,12z}$ and $H_{205y,12z}$, respectively).

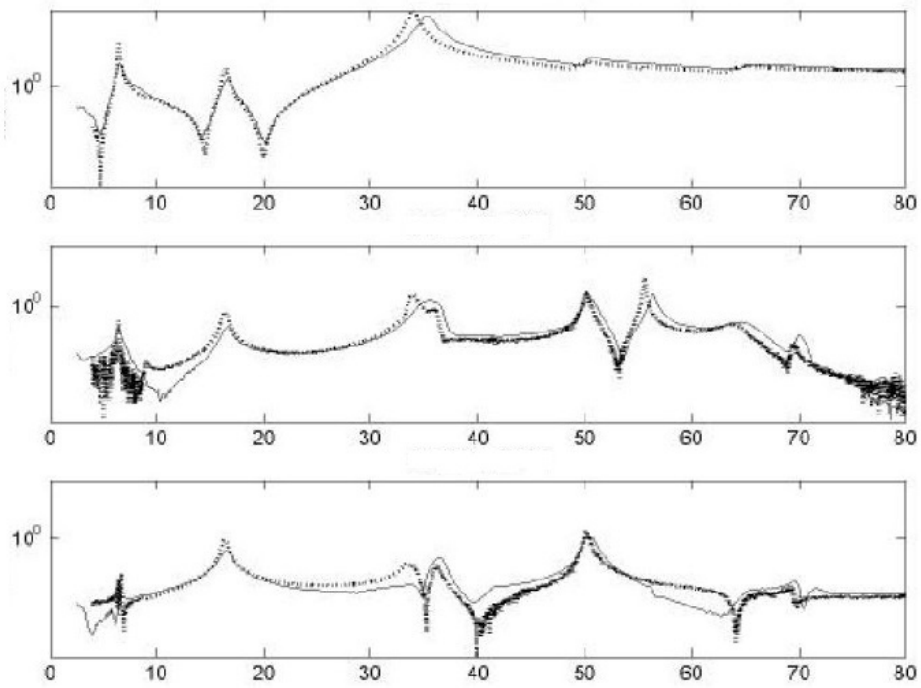

Figure 4.27: Frequency Response Functions measured by **U_MAN** (dashed lline) and **IC** (full line): $H_{12z,12z}$ (top), $H_{112x,12z}$ (middle) and $H_{205y,12z}$ (bottom)

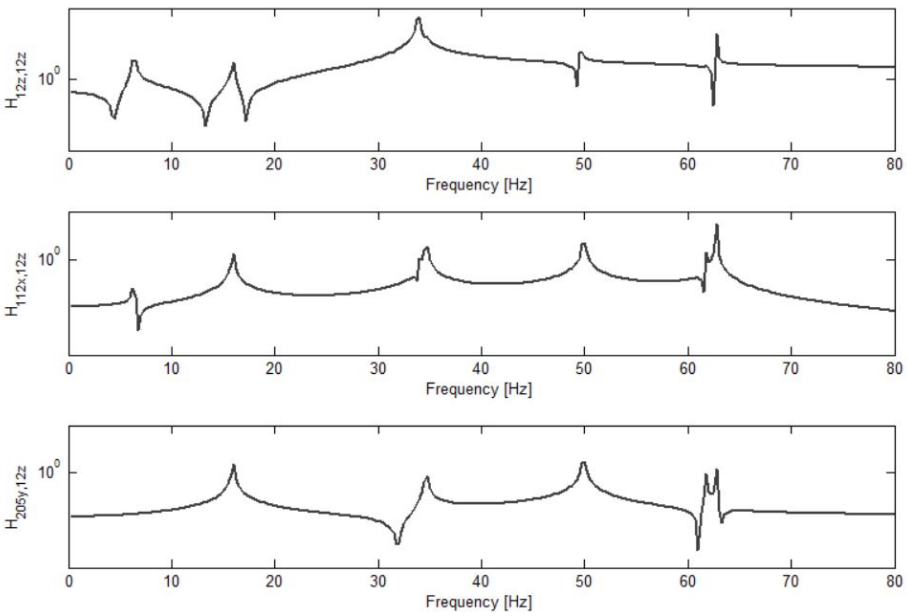

Figure 4.28: Frequency Response Functions obtained numerically

The FRFs curves presented serve only as a means of visually comparison between the test data available and the results obtained numerically. Observing more carefully, one can see that, even thought for lower frequency values the numerical FRFs amplitude values appear to be a better fit to the corresponding experimental values, for higher frequency values there is an obvious discrepancy between the two in terms of the location of the frequencies of resonance (FRFs peaks).

A more thorough analysis in terms of model updating could have been performed using the available modal data as reference. However, this analysis would fall out of the scope of this work.

The major objective with this analysis was to conclude about the accuracy of a model like the one used in this section, in terms of its predictive capabilities for a real simplified aircraft structure.

Even thought the FE model uses simple beam elements, comparing the numerical mode shapes and corresponding eigenfrequencies obtained numerically and experimentally, one can at least conclude that the results obtained for a lower frequency range are quite satisfactory, with eigenfrequency errors of about $2\,\%$.

With this analysis, the FE method applied to a simplified aircraft structure, using simple beam elements, was somehow verified and validated. Therefore, a similar FE model is applied to the experimental problem presented in the next section.

4.4 Experimental Simplified Aircraft Model Updating

For this last problem the model updating procedure based on the FRF and TR correlation functions is applied to a simplified aircraft structure, as presented in figure 4.29. Analogously, simple beam elements are used to model this structure.

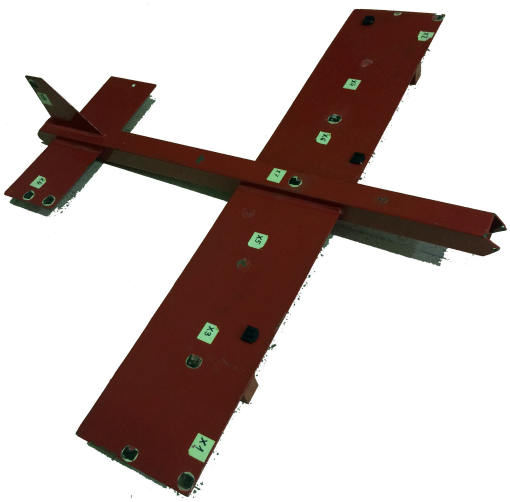

Figure 4.29: Experimental aircraft model

In the following sections the generated FE model is presented and a detailed analysis of the extracted experimental data will be performed in order to conclude about the best FRF curves to use in the model updating simulations. Finally, the updating simulations using the FRF and TR experimental data will be used to update the numerical model, using one and two updating parameters simultaneously.

4.4.1 Experimental Aircraft Numerical Model

It was concluded in the previous section 4.3 that, despite using simple beam elements to model the aircraft structure, the results obtained were quite good especially for low frequency values. This

conclusion is extrapolated to this problem, meaning that this aircraft structure will also be modeled using simple beam elements. Ultimately, one may conclude that the results obtained are accurate enough and suited to the proposed objectives, therefore validating this approximation.

The material assumed for this structure was a standard steel, with the properties presented in table 4.20.

Material Properties	
Young's modulus - E	$200\,GPa$
Density - ρ	$7870\,kgm^{-3}$
Poisson ratio - ν	0.3
Shear coefficient - k	$5/6$

Table 4.20: Experimental aircraft material properties

The FE model was generated using ANSYS with 30 FEs and 31 nodes (see figure 4.30). The elements are two-node 3D Timoshenko beam elements. Each node has six DOF $(u_x, u_y, u_z, \theta_x, \theta_y, \theta_z)$.

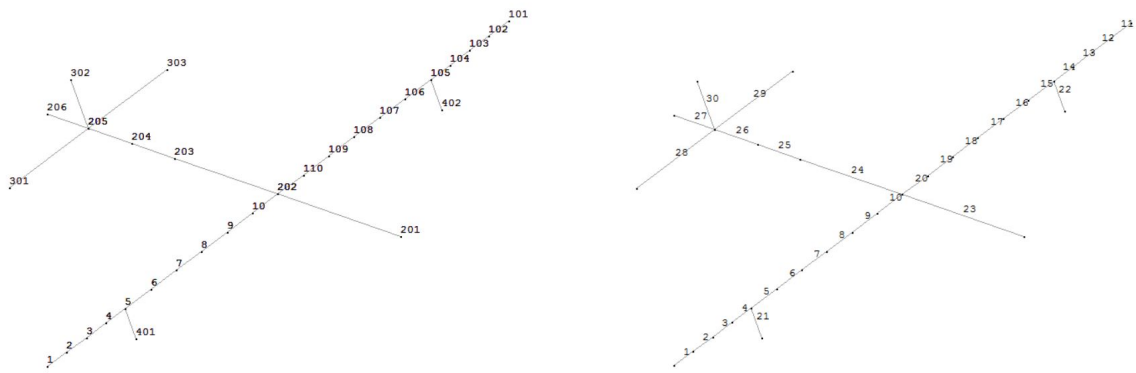

Figure 4.30: ANSYS FE model and nodes (left) and elements (right) numbering schemes for the experimental aircraft

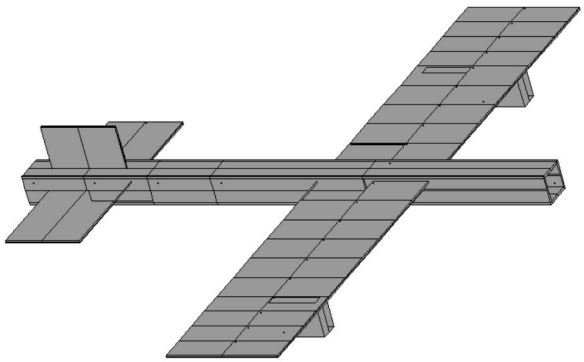

Figure 4.31: ANSYS FE model scheme for experimental aircraft

In order to simplify the updating simulations, the aircraft structure was divided into five major regions. Figure 4.31 presents the numbering schemes for the nodes and elements of the aircraft structure. Region 1 correspond to the aircraft wing (elements $1-20$) and region 3 to the fuselage (elements $23-27$). The fuselage cross section is hollow and has a thickness of $t = 0.0025\,m$. Region 2 are the aircraft "engines" (elements 21 and 22). Note that these two beam elements do not cover the all width of the main wing, and are positioned approximately at 30% of the wing in respect to the wing tip. Regions 4 and 5 correspond to the the horizontal tail and vertical tail (elements $28-29$ and 30), respectively.

The measured cross section width and height and beam lengths corresponding to each of the mentioned regions, are presented in the table 4.21.

Region	**b (m)**	**h (m)**	**L (m)**
1 (wing)	0.12	0.0025	0.65
2 ("engines")	0.1	0.02	0.037
3 (fuselage)	0.031	0.03	0.561
4 (horizontal tail)	0.08	0.0025	0.222
5 (vertical tail)	0.08	0.0025	0.06

Table 4.21: Dimensions of lengths (L), section width (b) and height (h) of the five aircraft regions

The FE model presented above, is the reference model for the following updating simulations.

4.4.2 Measurements Coherence

For the FRFs data extracted experimentally, a frequency range of $400\,Hz$ was considered while obtaining these values with a frequency interval increment of $0.5\,Hz$. However, for the updating simulations that follow, the active frequency range is $[0\,Hz, 80\,Hz]$, the same as the one considered in the previous problem in section 4.3.

The FRF curves obtained experimentally were $H_{1z,1z}$, $H_{101z,1z}$, $H_{1z,101z}$, $H_{101z,101z}$, $H_{1z,202z}$ and $H_{101z,202z}$, where z indicates the direction of the excitation or the accelerometer for each node considered.

As mentioned in section 3.2.2, five different measurements are taken to obtain one single FRF curve. The final measurement coherence curves for each FRF curve extracted, are presented in figure 4.32.

These coherence curves give us a close idea of the quality of the FRF curve extracted. Knowing that 1 correspond to perfect correlation and 0, no correlation at all, a coherence close to 1 in a certain frequency interval means that all five measures were consistent for the considered frequencies and therefore the corresponding FRF values are a relatively accurate representation of the physical system being studied.

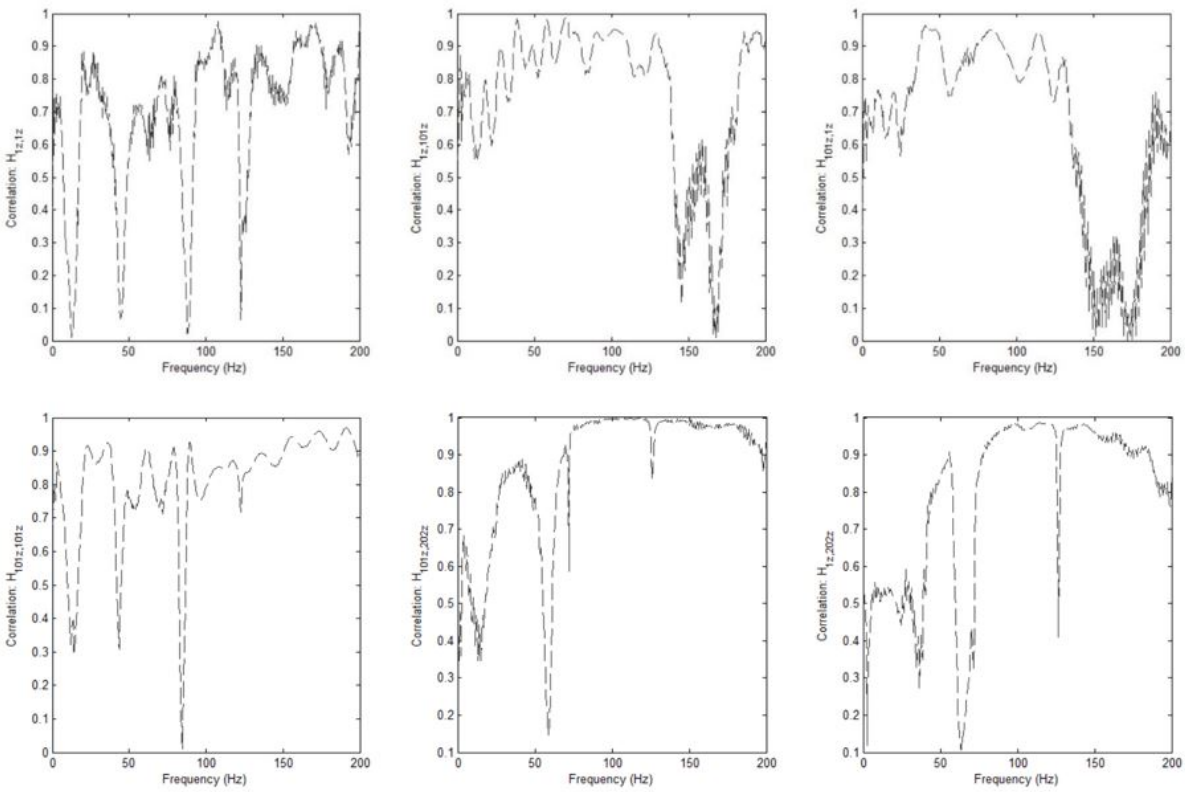

Figure 4.32: Experimental coherence curves of the measured frequency response functions

In general, one can observe that the values of correlation are slightly higher for lower frequency values up to a limit of about $100\,Hz$, except for the FRF $H_{1z,1z}$. This is related with the excitation technique used (impact hammer).

The best FRF curves within the frequency range of interest are $H_{1z,101z}$ and $H_{101z,1z}$. However, since these two curves have the exact same shape, we will be using only the $H_{101z,1z}$ FRF curve for updating purposes. The curve $H_{1z,101z}$ will also be presented in the results for each updating simulation, but only as a reference to the updating procedure.

4.4.3 Frequency Response Functions Model Updating

In this section the updating procedure developed based on the FRF correlation functions will be applied to this aircraft structure. The main objective here is to conclude about the applicability of this procedure to this aircraft structure and discuss the different results obtained using one and two updating parameters simultaneously.

The parameters considered for updating purposes are the global Young's modulus E and the length of the main wing L_1.

For the updating parameters considered in each updating simulation, the the initial and limit values are presented in the table 4.22 below. The values of the parameters not being updated in each simulation, are its corresponding reference values as presented in the sections above.

	Initial	Lower limit	Upper limit
$L_1\,(m)$	0.60	0.52	0.78
$E\,(GPa)$	210	160	240

Table 4.22: Initial and limit L_1 and E experimental aircraft

The model corresponding to the reference model with the initial modifications of the updating parameters of interest, is referred to as the initial model.

Model Updating Using One Updating Parameter

The parameters mentioned above will all be used to update the initial model individually, given the corresponding initial and limit values presented above.

The final updated values of each parameters considered as well as the difference relative to the corresponding reference values, are presented in table 4.23.

	Reference	Updated	$\Delta_{rel}\,(\%)$
$L_1\,(m)$	0.65	0.671	3.25
$E\,(GPa)$	200	177.19	-11.41

Table 4.23: Final updated values of L_1 and E separately, and reference deviation (%), FRF updating

The initial, experimental and updated final FRF curves for both $H_{101z,1z}$ and $H_{101z,101z}$ amplitude values, as well as the initial and final correlation functions for the updating of the wing length L_1, are presented in figures 4.33 and 4.34, respectively.

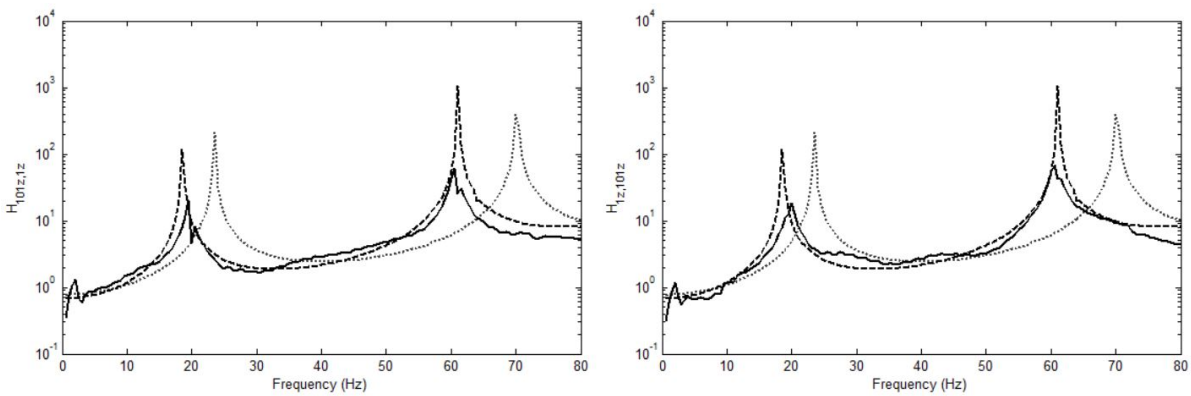

Figure 4.33: Initial (dotted line), experimental (full line) and updated (dashed line) $H_{101z,1z}$ (left) and $H_{101z,101z}$ (right), FRF updating of L_1

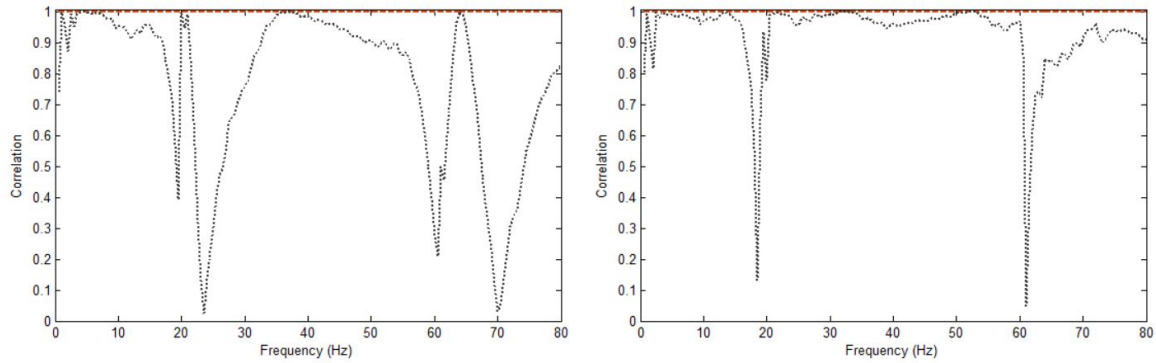

Figure 4.34: Initial (left) and final (right) correlation functions $CSAC(\omega)$ (orange dashed line) and $CSF(\omega)$ (black dotted line), FRF updating of L_1

The same curves obtained for the updating of the global Young's modulus E, are presented in both figures 4.35 and 4.36.

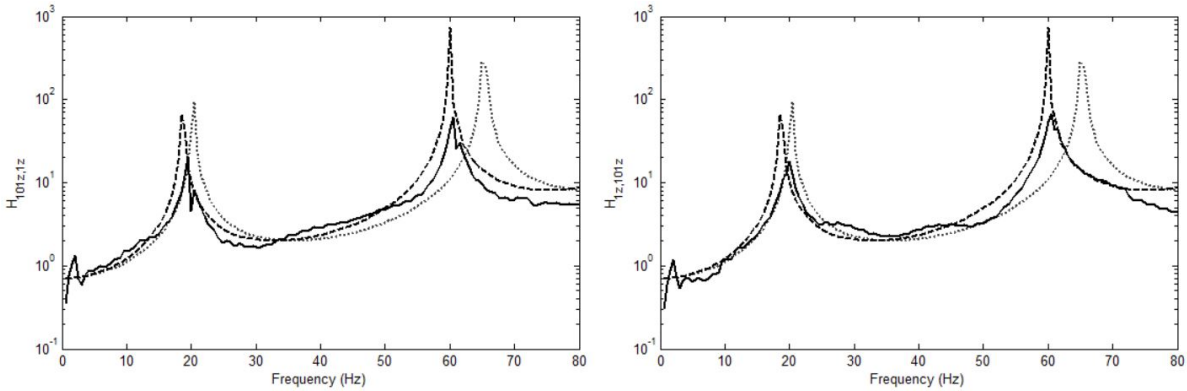

Figure 4.35: Initial (dotted line), experimental (full line) and updated (dashed line) $H_{101z,1z}$ (left) and $H_{101z,101z}$ (right), FRF updating of E

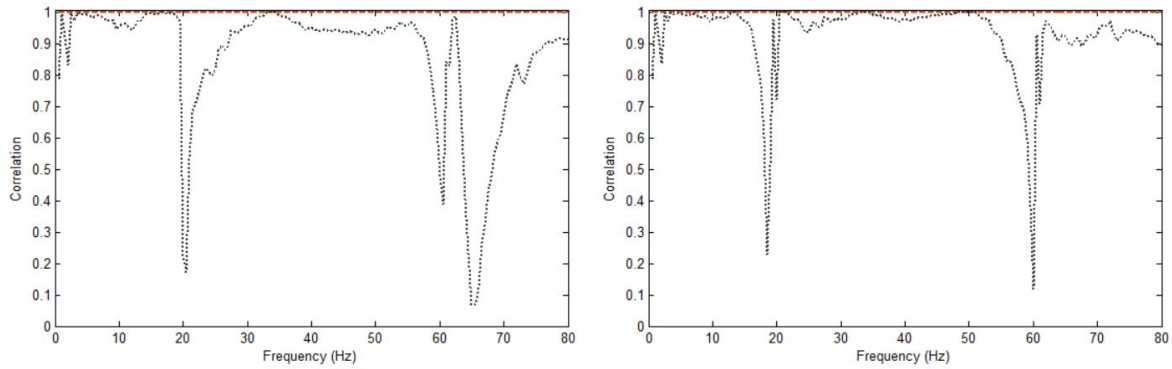

Figure 4.36: Initial (left) and final (right) correlation functions $CSAC(\omega)$ (orange dashed line) and $CSF(\omega)$ (black dotted line), FRF updating of E

As it was explained in section 2.6, when the column vector of either FRFs or TR functions is reduced to a scalar, the shape correlation function $CSAC(\omega)$ returns 1 across the full spectrum of frequencies even for uncorrelated FRFs or TR functions. Since we are only using one FRF to evaluate the correlation, it can be observed that $CSAC(\omega) = 1$ in the frequency range of interest.

Nevertheless, comparing the initial and final $H_{101z,1z}$ FRF curves, one can conclude that the updating procedures works as intended, as it can also be verified with the initial and final correlation curves, which indicates a clear increase in the overall correlation between the numerical and experimental data.

As expected, the FRF $H_{101z,101z}$ final curve, also fits adequately the experimental data.

Model Updating Using Two Updating Parameters

The updating procedure will now be tested using two updating parameters simultaneously considering the same initial and limit values presented in table 4.22. The values of the final updated parameters as well as the difference relative to the corresponding reference values, are presented next in table 4.24.

	Reference	**Updated**	$\Delta_{rel}\,(\%)$
$L_1\,(m)$	0.65	0.68125	4.81
$E\,(GPa)$	200	206.875	3.438

Table 4.24: Final updated values of L_1 and E simultaneously, and reference deviation (%), FRF updating

The initial, experimental and updated final FRF curves for both $H_{101z,1z}$ and $H_{101z,101z}$ amplitude values, as well as the initial and final correlation functions for the simultaneous updating of L_1 and E, are presented in figures 4.37 and 4.38, respectively.

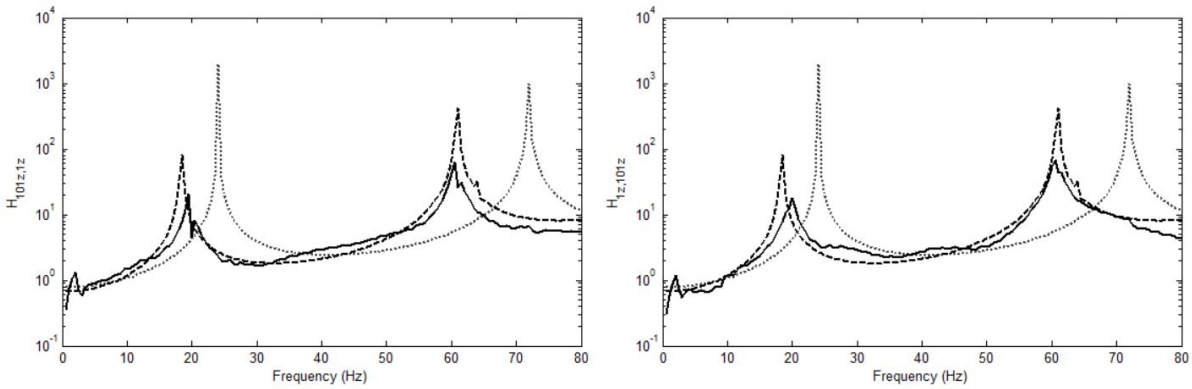

Figure 4.37: Initial (dotted line), experimental (full line) and updated (dashed line) $H_{101z,1z}$ (left) and $H_{101z,101z}$ (right), FRF updating of L_1 and E

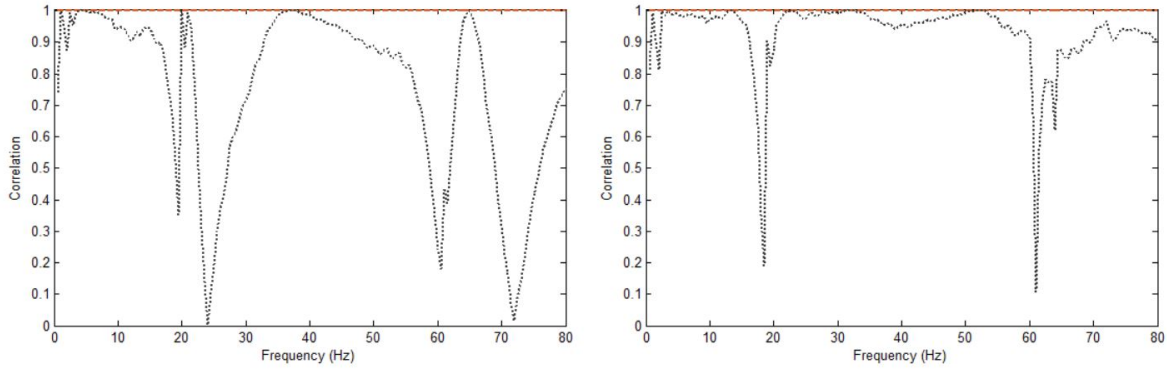

Figure 4.38: Initial (left) and final (right) correlation functions $CSAC(\omega)$ (orange dashed line) and $CSF(\omega)$ (black dotted line), FRF updating of L_1 and E

Once again, one can verify that using two updating parameters simultaneously, this updating procedure works rather effectively and gives us the expected results.

Despite some obvious amplitude discrepancies at resonance frequencies as presumably justified by the absence of damping in the numerical results, the curve shape of the final and experimental FRF curves are significantly similar, at least visually, and present good correlation.

The final correlation function $CSF(\omega)$ clearly indicates these amplitude discrepancies close to the resonance peaks. However, one can verify the overall and significant increase in this correlation function values throughout the frequency range considered.

Whether updating the wing length L_1 individually or together with the E, the final updated value for is parameter presents a difference in respect to the reference value of approximately 4.5% in both cases, which is fairly adequate.

4.4.4 Transmissibility Model Updating

The model updating procedure based on the TR correlation functions will now be tested using one and two updating parameters simultaneously applying the TR model updating procedure.

The updating parameters used in the next simulations are the sames ones used in the previous section, the wing length L_1 and the global Young's modulus E.

The initial and limit values (see section 3.1.3) applied to each updating simulation performed in this section, are the same as in the previous and are presented in table 4.22.

Analogously to what was done in the previous section, only one TR curve will be considered during the updating process. This will lead once again to the case where the correlation function $CSAC(\omega)$ assumes the values 1 throughout the frequency range considered. The curve used in the updating procedure will be $T_{1z,202z}$. The curve $T_{101z,202z}$ will also be presented in the results for comparison purposes only.

Model Updating Using One Updating Parameter

The results for each of the simulations performed updating each parameter individually are present in the table 4.25.

	Reference	**Updated**	$\Delta_{rel}\,(\%)$
$L_1\,(m)$	0.65	0.6603	1.585
$E\,(GPa)$	200	188.75	-5.625

Table 4.25: Final updated values of L_1 and E separately, and reference deviation (%), TR updating

The initial, experimental and updated final TR curves for both $T_{1z,202z}$ and $T_{101z,202z}$ amplitude values, as well as the initial and final correlation functions for the updating of the wing length L_1, are presented in figures 4.39 and 4.40, respectively. The corresponding curves obtained for the updating of the global Young's modulus E, are presented in figures 4.41 and 4.42.

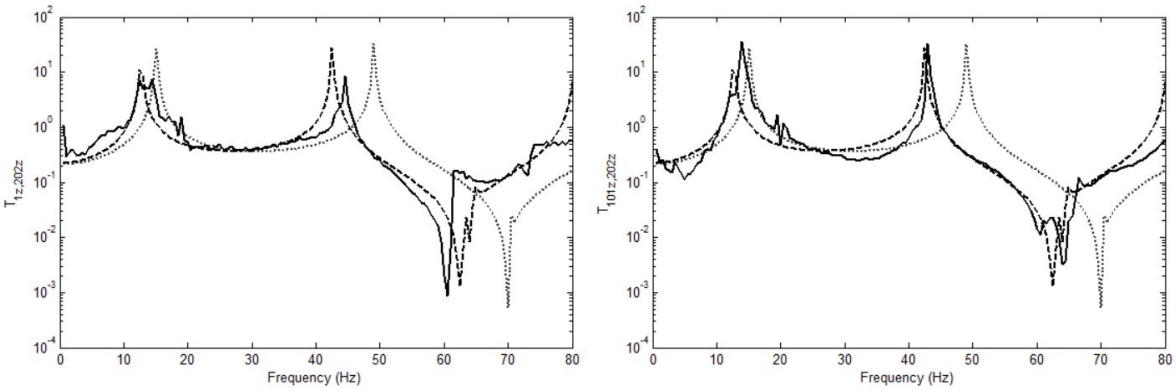

Figure 4.39: Initial (dotted line), experimental (full line) and updated (dashed line) $T_{1z,202z}$ (left) and $T_{101z,202z}$ (right), TR updating of L_1

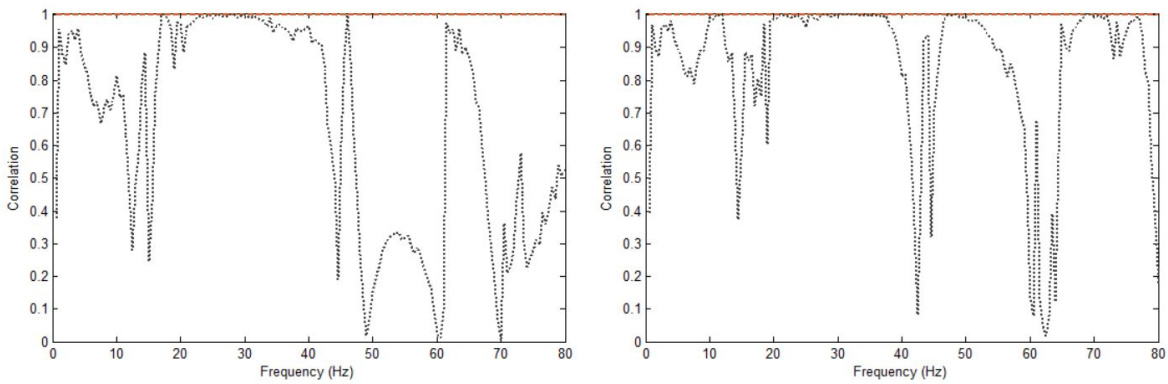

Figure 4.40: Initial (left) and final (right) correlation functions $CSAC(\omega)$ (orange dashed line) and $CSF(\omega)$ (black dotted line), TR updating of L_1

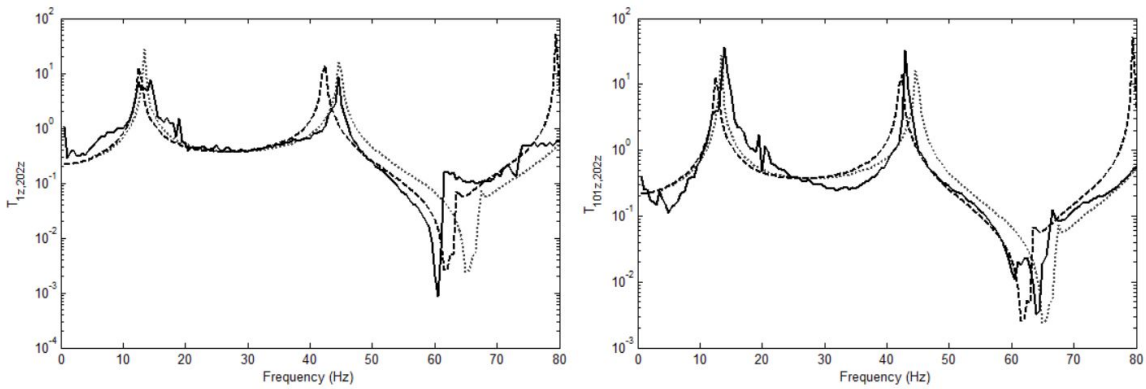

Figure 4.41: Initial (dotted line), experimental (full line) and updated (dashed line) $T_{1z,202z}$ (left) and $T_{101z,202z}$ (right), TR updating of E

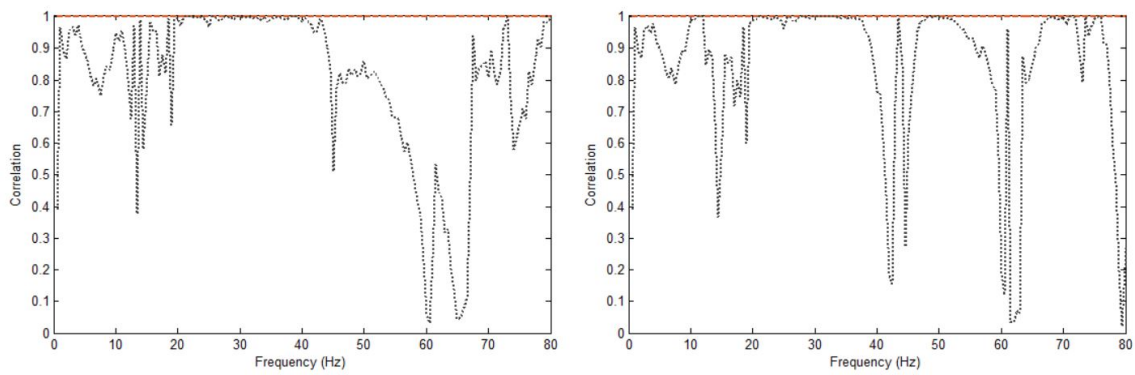

Figure 4.42: Initial (left) and final (right) correlation functions $CSAC(\omega)$ (orange dashed line) and $CSF(\omega)$ (black dotted line), TR updating of E

Comparing the final updated results obtained here with the results obtained using the FRF procedure, one can verify a clear convergence of the final updated results. More importantly the difference between the measured and updated main wing length L_1, is also quite acceptable, indicating an increase of just 1.585% in respect to its reference measured value.

Model Updating Using Two Updating Parameters

Using the same updating parameters to update our initial FE model simultaneously, the following results, presented in table 4.26.

	Reference	**Updated**	$\Delta_{rel}\,(\%)$
$L_1\,(m)$	0.65	0.6231	-4.128
$E\,(GPa)$	200	161.95	-19.02

Table 4.26: Final updated values of L_1 and E simultaneously, and reference deviation (%), TR updating

The initial, experimental and updated final TR curves for both $T_{1z,202z}$ and $T_{101z,202z}$ amplitude values, as well as the initial and final correlation functions for the updating of the wing length L_1, are presented

in figures 4.43 and 4.44, respectively.

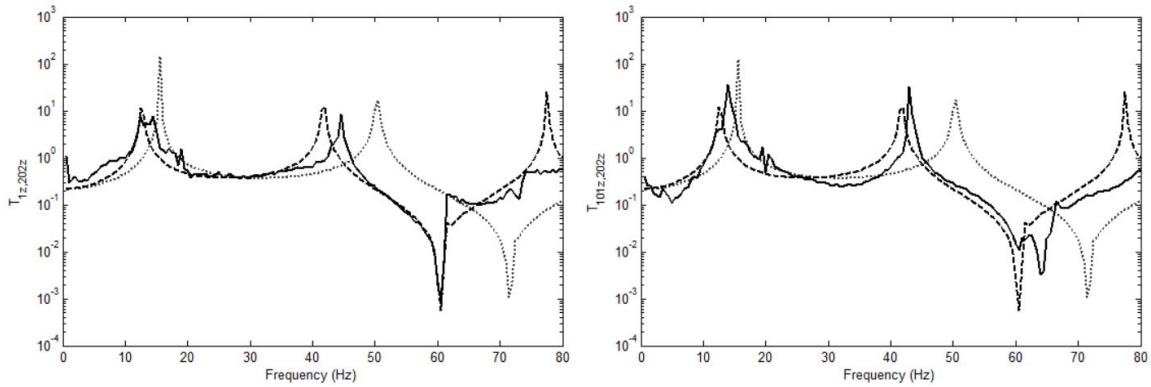

Figure 4.43: Initial (dotted line), experimental (full line) and updated (dashed line) $T_{1z,202z}$ (left) and $T_{101z,202z}$ (right), TR updating of L_1 and E

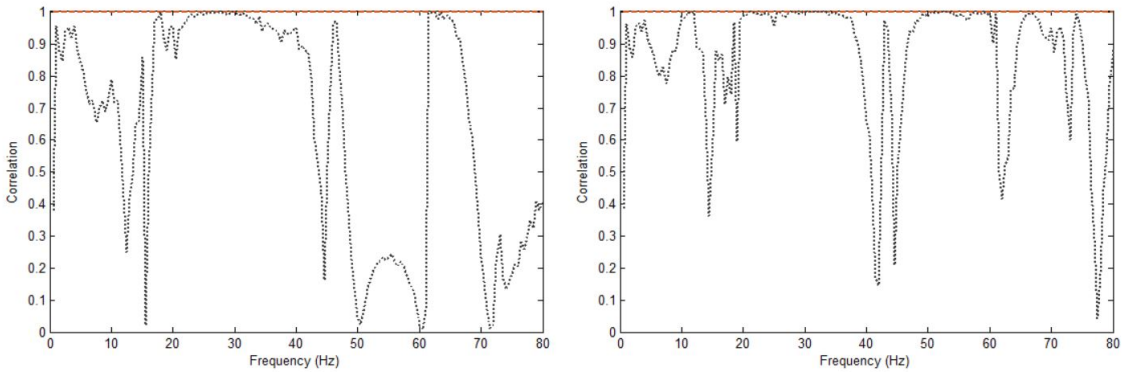

Figure 4.44: Initial (left) and final (right) correlation functions $CSAC(\omega)$ (orange dashed line) and $CSF(\omega)$ (black dotted line), TR updating of L_1 and E

The TR and correlation graphs presented above indicate a visible increase in the correlation between the updated and experimental data. These results obtained here are relatively different when compared with the results updating the two parameters simultaneously using the FRF updating procedure. Nevertheless, the wing length L_1 value, keeps a difference in respect to the measured wing length, of approximately 4%.

Concluding, the confidence in the final updated results obtained is highly dependent on the quality of the experimental data used in the updating procedures, and also very important is the selection of the updating parameters.

It is important to note that for the updating of the aircraft structure, the final updated value of E when updated individually using the FRF-based technique, and when updated simultaneously together with the wing length L_1 using the TR-based updating technique, is significantly low considering it is a steel structure, which was the material assumed. This can be a clear indication that the selected updating parameter E might not be the most appropriated to apply to this aircraft structure. This suggests that further investigation could have been done in terms of testing different updating parameters of the aircraft structure.

Chapter 5

General Conclusions and Suggestions for Future Work

Model updating can be defined as the systematic adjustment of model parameters in order to reduce the discrepancies between the numerical and experimental data.

Response-based model updating techniques have proven through the years to be far more attractive than the modal-based updating formulations. These conventional model updating techniques make use of measured frequency response functions and modal parameter estimates to update the FE model parameters.

In recent years, some investigation have been done in the field of model updating concerning the application of TR experimental data for updating purposes.

This work presents a model updating technique in which the experimental TR measurements are used in the updating procedure. The measured TR functions described are defined as the ratio between two (measured) responses assuming the location of the force is known.

The results obtained using the FRF and TR based updating techniques show that both methodologies implemented are able to adjust the updating parameters so that the discrepancies between the considered numerical and experimental data are significantly reduced.

In order to perform this adjustment in a physically meaningful way, rather than just updating the numerical model mathematically, it was also verified that the success of the updating procedure is highly dependent on the correct selection of the updating parameters and the limitation of these parameters in the updating routine. That is, the selected numerical data may be adjusted to the corresponding experimental data, but the adjusted updating parameters, such as a measured thickness or material density, are excessively modified in a way that the final model loses its physical meaning. In order to avoid this problem, the optimization in the updating procedure has to be constrained so that the final values of the selected updating parameters are limited within the defined range of values. Applying these constraints to the updating parameters also improve the computational efficiency of the updating procedure, by reducing the number of iterations of the optimization routine.

The optimization procedure was defined using the Cross Signature Correlation functions (CSC). The

two correlation functions considered (CSAC and CSF) allow the correlation of any number of measurements and their corresponding predictions in a consistent manner, in a way that these amplitude and shape correlation functions can measure the closeness between two corresponding FRFs or TR functions, at any frequency point and return a value between zero and one.

The analysis of the final FRF or TR curves was mostly done by visual inspection, although the correlation functions turn this inspection easier. Nevertheless, in order to increase the visual perception of the quality of the updating procedure, the initial and final correlation functions were also presented for each updating simulation performed.

Analysing the updating results obtained in each experimental case, in terms of the final updating parameter estimates, one can verify that these values are not unique. In fact, it can be observed that these estimates not only vary with the number of modes used to calculate the FRF values (verified in the case of FRF-based model updating), but also and more evidently it vary with the number of updating parameters used. Comparing the updating results obtained using the two updating methodologies implemented, it can also be seen that these parameter estimates are not unique and are also dependent on the updating procedure employed and the experimental data used.

Despite the fact that the final parameter estimates, using both methodologies, are very close and within an acceptable range of values in respect to its reference values, one can only conclude that both methodologies work according to the expected, visibly reducing the discrepancies between the experimental and numerical responses.

For the aircraft structure, one can verify that the final parameter estimate of the Young modulus E, for either the FRF-based or the TR-based updating methodologies, fluctuate considerably. For example, for the TR-based updating, this parameter updated individually assumes a final value of $188.75\ GPa$, and for the updating simultaneously with the wing length L_1, it assumes a final value of $161.95\ GPa$, which is too low for a steel.This fact can be seen as an indication that the selected parameters to the updating procedure might not have been the most appropriate.

In terms of the FE methodology employed in this work, it can be verified that, despite the simple FE methodology used for the experimental aircraft using beam elements, the results obtained are in concordance with the measured data, specially for a low range of frequency.

As a suggestion for future work, I propose the development of an alternative FE model updating methodology based on the directly measured force TR functions. The optimization procedures could be improved in terms of computational performance, and the global updating procedure could be formulated using a different objective function in which the analytical TR functions are updated directly rather than indirectly by updating the correlation functions. Future work concerning the experimental aircraft model presented in this thesis should include the effect of damping.

Bibliography

[1] J.E. Mottershead, and M.I. Friswell. Model Updating In Structural Dynamics: A Survey. *Journal of Sound and Vibration*, 167(2):347–375, 1993.

[2] E. Dascotte and J. Strobbe. Updating Finite Element Models Using FRF Correlation Functions. *Proceedings of the 17th IMAC Conference, Kissimmee, Florida*, page 1169–1174, 1999.

[3] G. Steenackers, C. Devriendt, and P. Guillaume. On the Use of Transmissibility Measurements for Finite Element Model Updating. *Journal of Sound and Vibration*, 303(3-5):707–722, 2007.

[4] B. Goller, M. Broggi, A. Calvi and G. Schuëller. A stochastic model updating technique for complex aerospace structures. *Finite Elements in Analysis and Design*, 47(7):739–752, 2011.

[5] Space engineering: Structural general requirements, nov 2008. ECSS-E-ST-32C Rev. 1.

[6] M. Brughmans, J. Leuridan, G. Hrycko and J. Wyzykowski. Application of FEM Model Correlation and Updating Techniques on an Aircraft Using Test Data of a Ground Vibration Survey. 1991.

[7] M. Link, B. Staples, D. Göge, M. Böswald and Th. Boettcher. Linking Analysis to Test - Parameter Identification and Validation. In *Proceedings of the 29rd International Seminar on Modal Analysis (ISMA23), Leuven, Belgium*, 2004.

[8] C. Schedlinski, M. Link and A. Schönrock. Application of Computational Model Updating to Aeroengine Components. In *Proceedings of the 29rd International Seminar on Modal Analysis (ISMA23)*, 2004.

[9] A.P. Boresi and R.J. Schmidt. *Advanced Mechanics of Materials*. Wiley, 1993.

[10] S. Timoshenko and J.N. Goodier. *Theory of Elasticity*. McGraw-Hill, 1970.

[11] Martin H. Sadd. *Elasticity Theory: Applications and Numerics*. Elsevier Butterworth Heinemann, 2005.

[12] L. Majkut. Free and Forced Vibrations of Timoshenko Beams Described by Single Difference Equation. *Jornal of Theoretical and Applied Mechanics*, page 193–210, 2009.

[13] O. C. Zienkiewicz and R. L. Taylor. *The Finite Element Method*. Butterworth-Heinemann, 2000.

[14] P. Lagos. Caracterização da Resposta de Vibração de um Exaustor. *Universidade de Lisboa, Instituto Superior Técnico*, 2016.

[15] J. N. Reddy. *An Introduction to the Finite ElementMethod*. McGraw-Hill, 1993.

[16] H. Grafe. *Model Updating of Large Structural Dynamics Models Using Measured Response Functions*. PhD thesis, Imperial College of Science, Technology and Medicine University of London, oct 1998.

[17] I. Newton. *Philosophiae Naturalis Principia Mathematica*. 1686.

[18] D. J. Ewins. Modal testing: Theory and practice. letchworth. *Research Studies Press.*, 1984.

[19] R.E. Spears and S.R. Jensen. Approach for Selection of Rayleigh Damping Parameters Used for Time History Analysis. *Volume 8: Seismic Engineering*, 2009.

[20] W. Liu and D.J. Ewins. Transmissibility Properties of MDOF Systems. *16th International Modal Analysis Conference (IMAC) - Model Updating and Correlation*.

[21] N. M. M. Maia, A. P. V. Urgueira, and R. A. B. Almeida. Whys and Wherefores of Transmissibility. *Vibration Analysis and Control - New Trends and Developments*, Jun 2011.

[22] Y.E. Lage, M.M. Neves, N.M.M. Maia, and D. Tcherniak. Force Transmissibility Versus Displacement Transmissibility. *Journal of Sound and Vibration*, 333(22):5708–5722, 2014.

[23] Y. E. Lage, N. M. M. Maia, and M. M. Neves. Force Magnitude Reconstruction Using the Force Transmissibility Concept. *Shock and Vibration*, 2014:1–9, 2014.

[24] Mathworks, moore-penrose pseudoinverse of matrix. `https://www.mathworks.com/help/matlab/ref/pinv.html`.

[25] G. Steenackers. *Finite Element Model Updating and Optimization of Mechanical Systems Making Use of Regressive Techniques*. PhD thesis, Vrije Universiteit Brussel, may 2008.

[26] M. I. Friswell and J. E. Mottershead. Finite Element Model Updating in Structural Dynamics. *Kluwer Academic Publisher*, 1999.

[27] V. Arora. Use of Resonance and Antiresonance Frequencies for better Matching of Frequency Response Function. *International Journal of Structural Engineering*, 5(1):13, 2014.

[28] J. Bös. Numerical Optimization of the Thickness Distribution of Three-Dimensional Structures with Respect to their Structural Acoustic Properties. *Structural and Multidisciplinary Optimization*, 32(1):12–30, 2006.

[29] *Optimization toolbox for use with MATLAB: user's guide*. The Math Works, 2004.

[30] G. Steenackers and P. Guillaume. Finite Element Model Updating Taking into account the Uncertainty on the Modal Parameters Estimates. *Journal of Sound and Vibration*, 296(4-5):919–934, 2006.

[31] R. Allemang and D. Brown. A correlation coefficient for modal vector analysis. In *1st International Modal Analysis Conference, Orlando, USA*, 1984.

[32] W. Heylen and S. Lammens. FRAC: a Consistent Way of Comparing Frequency Response Functions. In *Identification in Engineering Systems, Proceedings at Swansea*, mar 1996.

[33] Z. Xu, H. Hua, R. She and G.Z. Wang. Updating Large Structure Model by the Sensitivity Analysis of FRF Correlation Functions. *JSME Int. J., Ser. C JSME International Journal Series C*, 46(1):145–149, 2003.

[34] ANASYS INC. *ANSYS Parametric Design Language Guide*.

[35] N. Teunisse. Interactive Link Between MATLAB and ANSYS. `https://www.mathworks.com/matlabcentral/fileexchange/53032-interactive-link-between-matlab-and-ansys`, 2015.

[36] M. Carvalho J.L. Vale L.T. Pinheiro and M.M. Neves. Techniques adopted in integrating structural analysis with numerical optimization. *5th International Conference on Mechanics and Materials in Design, At Porto, Volume: Chapter II: Structural and Multidisciplinary Optimization in Design*.

[37] M. Skeen and G. Lucas. *Brüel Kjær Pulse Labshop Primer*.

[38] J.D. Renton. Generalized Beam Theory Applied to Shear Stiffness. *International Journal of Solids and Structures*, 27(15):1955–1967, 1991.

[39] M. Link and M. Friswell. Working Group 1: Generation Of Validated Structural Dynamic Models—Results Of A Benchmark Study Utilising The Garteur Sm-Ag19 Test-Bed. *Mechanical Systems and Signal Processing*, 17(1):9–20, 2003.

[40] A. Gravalle. *Ground Vibration Test Techniques*. 1999.

Appendix A

Solution of the Equations of Vibration of the Timoshenko Beam Element

The demonstration presented next follows the exact same notation and train of thought of the paper [12]. The solution presented is only valid up to a frequency limit of $\omega < \sqrt{(GkA)/(\rho I)}$.

The set of coupled differential equations for transverse vibration of uniform Timoshenko beam with a constant cross section are given by:

$$\frac{\partial}{\partial x}\left[kGA\left(\frac{\partial y(x,t)}{\partial x} - \Theta(x,t)\right)\right] = \rho A\frac{\partial^2 y(x,t)}{\partial t^2} - q(x,t) \tag{A.1}$$

$$kGA\left(\frac{\partial y(x,t)}{\partial x} - \Theta(x,t)\right) - \frac{\partial}{\partial x}\left(EI\frac{\partial \Theta(x,t)}{\partial x}\right) = I\rho\frac{\partial^2 \Theta(x,t)}{\partial t^2} \tag{A.2}$$

where: k - Timoshenko shear coefficient depending on the cross section of the beam, G - shear modulus, A - cross sectional area, E - Young modulus, I - second moment of area, ρ - density and $q(x,t)$ the external force.

The functions that give the solution of these equations are the vibration amplitude $y(x,t)$, and the angle due to pure bending $\Theta(x,t)$.

Employing the Fourier method of variable separation, it is assumed that each function $y(x,t)$ and $\Theta(x,t)$ can be presented in the form of a product of a function dependent on the spacial coordinate x and a function dependent on time t:

$$y(x,t) = X(x)\,T(t) \qquad\qquad \Theta(x,t) = Y(x)\,T(t) \tag{A.3}$$

After several simple transformations of the system presented in equations A.1 and A.2, it can be written as:

$$\begin{aligned} &X''(x) + a(x) - Y'(x) = 0 \\ &Y''(x) + bY(x) + cX'(x) = 0 \\ &\ddot{T}(t) + \omega^2 T(t) = 0 \end{aligned} \tag{A.4}$$

where

$$a = \frac{\omega^2 \rho}{kG}; \qquad b = \frac{\rho\omega^2}{E} - c; \qquad c = \frac{GkA}{EI} \tag{A.5}$$

and ω is the vibration frequency.

By eliminating the function $Y(x,t)$ from the two first equations of the system A.4 (see equation A.6), one can get an equation for the transverse displacement $X(x)$. The equation for the free vibration of Timoshenko beam, can be expressed as presented in equation A.7.

$$Y(x) = -\frac{1}{b}\left[X'''(x) + (a+c)X'(x)\right] \tag{A.6}$$

$$X^{(4)}(x) + dX''(x) + eX(x) = 0 \tag{A.7}$$

where

$$d = a + b + c = \frac{\omega^2 \rho I \left(1 + \frac{E}{Gk}\right)}{EI}; \qquad e = ab = \frac{\omega^2 \left(\omega^2 \rho^2 \frac{I}{Gk} \rho A\right)}{EI} \tag{A.8}$$

The characteristic equation of equation A.7 has the form:

$$r^4 + dr^2 + e = 0 \tag{A.9}$$

Replacing $r^2 = \tilde{z}$, roots of the characteristic equation are given by:

$$\tilde{z}_1 = \frac{1}{2}\left(-d + \sqrt{\Delta}\right) \qquad \tilde{z}_2 = \frac{1}{2}\left(d + \sqrt{\Delta}\right) \tag{A.10}$$

where

$$\Delta = d^2 - 4e = \omega^4 \rho^2 I^2 \left(1 - \frac{E}{kG}\right)^2 + 4EI\omega^2 \rho A \tag{A.11}$$

It is easily observed that $\Delta > 0 \; \forall \, \omega$. Analysing the signal of the roots $\tilde{z}_1$ and $\tilde{z}_2$:

$$\begin{aligned} &\tilde{z}_2 < 0 \qquad \forall \, \omega \\ &\tilde{z}_1 > 0 \qquad \Leftrightarrow \qquad \sqrt{d^2 - 4e} > d \qquad \Rightarrow \qquad e > 0 \quad for \quad \omega < \sqrt{\frac{GkA}{\rho I}} \\ &\tilde{z}_1 \qquad for \qquad \omega > \sqrt{\frac{GkA}{\rho I}} \end{aligned} \tag{A.12}$$

Since we are only interested in the solution for $\omega < \sqrt{\frac{GkA}{\rho I}}$, the roots for equation A.9 are given by:

$$r_1 = \sqrt{\tilde{z}_1} \qquad r_2 = -\sqrt{\tilde{z}_1} \qquad r_3 = \imath\sqrt{-\tilde{z}_2} \qquad r_4 = -\imath\sqrt{-\tilde{z}_2} \tag{A.13}$$

This gives a solution in the form:

$$X(x) = C_1 e^{\sqrt{\tilde{z}_1}x} + C_2 e^{-\sqrt{\tilde{z}_1}x} + C_3 e^{\imath\sqrt{\tilde{z}_2}x} + C_4 e^{-\imath\sqrt{\tilde{z}_2}x} \tag{A.14}$$

Using Euler's formulae, the solution presented in equation A.14 can be expressed in its trignometric form as presented in the equation A.15.

$$X(x) = P_1\ cosh(\lambda_1 x) + P_2\ sinh(\lambda_1 x) + P_3\ cos(\lambda_2 x) + P_4\ sin(\lambda_2 x) \tag{A.15}$$

where

$$\lambda_1^2 = |\tilde{z}_1| = \frac{-d + \sqrt{\Delta}}{2} \qquad \lambda_2^2 = |\tilde{z}_2| = \frac{d + \sqrt{\Delta}}{2} \tag{A.16}$$

The BC for a simply supported beam are given in equation A.17, at the supported end with the coordinate x_i:

$$y(x_i, t) = 0; \qquad EI\ \frac{\partial \Theta(x,t)}{\partial x} = 0 \tag{A.17}$$

After separation of variables and taking into consideration the equation A.6, considering the ends of the simply supported beam are located in $x = 0$ and $x = l$, we obtain the following BCs:

$$\begin{aligned} x = 0 \quad X(0) = 0 \quad and \quad X''(0) + aX(0) = 0 \\ x = l \quad X(l) = 0 \quad and \quad X''(l) + aX(l) = 0 \end{aligned} \tag{A.18}$$

where l represents the length of the beam.

From the BC at $x = 0$, the following equations are obtained:

$$P_1 + P_3 = 0 \qquad \lambda_1^2 P_1 - \lambda_2^2 P_2 = 0 \tag{A.19}$$

The system of equations presented in A.19 is satisfied when $P_1 = P_3 = 0$, or in the case when $\lambda_1^2 + \lambda_2^2 = 0$, .e. when $\sqrt{d^2 - 4e} = 0$, and this is possible only when $\omega = 0$, which describes motion of the beam as a rigid body, which is impossible given the BC.

Finally, given that the BCs at $x = 0$ require that $P_1 = P_3 = 0$, the BCs at $x = l$ are expressed by the matrix equation A.20 presented below:

$$\begin{bmatrix} sinh(\lambda_1 l) & sin(\lambda_2 l) \\ \lambda_1^2 sinh(\lambda_1 l) & -\lambda_2^2 sin(\lambda_2 l) \end{bmatrix} \begin{bmatrix} P_2 \\ P_4 \end{bmatrix} = \begin{bmatrix} 0 \\ 0 \end{bmatrix} \tag{A.20}$$

The nontrivial solution for this problem is obtained from the condition that the determinant of the main matrix presented above is equal to zero. This matrix will be referred to as matrix D:

$$D = \begin{bmatrix} sinh(\lambda_1 l) & sin(\lambda_2 l) \\ \lambda_1^2 sinh(\lambda_1 l) & -\lambda_2^2 sin(\lambda_2 l) \end{bmatrix} \tag{A.21}$$

$$det(D) = -(sinh(\lambda_1 l) \cdot \lambda_2^2 sin(\lambda_2 l) + \lambda_1^2 sinh(\lambda_1 l) \cdot sin(\lambda_2 l)) = 0 \tag{A.22}$$

The expression presented in equation A.22 allows us to calculate the natural frequencies ($\omega = 2\pi f$) of a simply supported beam according to the Timoshenko beam theory, keeping always in mind this result is only valid up to a frequency limit of $\omega = \sqrt{(GkA)/(\rho I)}$.

Appendix B

MATLAB Code - Analytical Natural Frequencies, Simply Supported Timoshenko Beam

This MATLAB code is divided in two different scripts, the main script *Timoshenko_Simply_Supported_Beam.m* and the function *matrixD.m*, which defines matriix D as presented in Appendix A.

The beam dimensions and elastic properties have to be defined at the beginning of the main script, as well as the frequency range of interest within which we want obtain all the natural frequencies of the simply supported Timoshenko beam.

The main script *Timoshenko_Simply_Supported_Beam.m* is presented below.

```
clear all
%%%%%%%%%%%%%%%%%%%%%%%%%%%%%%%%%%%%%%%%%%%%%%%%%%%%%%%%%%%%%%%%%%%%%%%
%This function calculates the first natural frequencies of the simply
%supported beam based on the beam Timoshenko theory (freq_nat) for a
%defined frequency range of interest, freq_r.
%%%%%%%%%%%%%%%%%%%%%%%%%%%%%%%%%%%%%%%%%%%%%%%%%%%%%%%%%%%%%%%%%%%%%%%%

freq_r=750; %frequency range o interest (Hz)
%%% Beam Properties %%%
E=211e09; %Young modulus (Pa)
L=0.975; %length(m)
h=0.02; %cross section height (m)
c=0.02; %cross section width (m)
A=c*h; %cross section area
rho=7870; %sensity (kgm^-3)
I=(c*(h^3))/12; %second moment of area
k=5/6; %Timoshenko shear coefficient
poisson=0.3; %Poisson coefficient
G=E/(2*(1+poisson)); %Shear modulus
```

```
j=1;
int=0.5;
x0 = int;
for i=1:1:freq_r/int
    [x fval exitflag output] = fzero( @(x) matrixD(x,E,rho,L,A,I,k,G), x0);
    x0 = x0+int;
    prel(i)=x
    %%% stores first natural frequency %%%
    if and(j==1, prel(i)>0)
        freq_nat(j)=x;
        j=j+1;
    end
    %%% stores natural frequencies from 2 to last before freq_r limite %%%
    if j>1
        if and( prel(i)>0, abs(prel(i) - freq_nat(j-1)) >1e-5 )
            freq_nat(j)=x;
            j=j+1;
        end
    end
end

freq_nat
```

Function *matrixD.m* is presented below.

```
function [ detD ] = matrixD( x,E,rho,L,A,I,k,G )

p_p2=(2*pi*x)^2;

a=(p_p2*rho)/(k*G);
c=(G*k*A)/(E*I);
b=((rho*p_p2)/E)-c;
d=a+b+c;
e=a*b;

Δ=d^2-4*e;

lab_1=sqrt(  (-d+sqrt(Δ))/2  );
lab_2=sqrt(  (d+sqrt(Δ))/2  );

detD=-(   sinh(lab_1*L)*(lab_2^2)*sin(lab_2*L)  +  (lab_1^2)*sinh(lab_1*L)*sin(lab_2*L) ...
      );

end
```